

UNIVERSITY OF KWAZULU-NATAL



**Dynamical Mass estimates of
Sunyaev-Zel'dovich Effect selected
Galaxy Clusters in the Millennium
Gas Simulations**

by

Nhlakanipho Kwazi Mthembu

Submitted in fulfilment of the
academic requirements for the degree of
Master of Science,
in the
School of Mathematics, Statistics, and Computer Science,
University of KwaZulu-Natal

Durban
June 2016

*Astronomy? Impossible to understand and
madness to investigate. - Sophocles, c. 420 BC*

Abstract

To extract and make estimates of the cosmological parameters requires knowledge of the cluster mass. Cluster mass is not directly observable but can be predicted by numerical simulations of structure formation and can be inferred from observable proxies for mass. One way to find a cluster is by the Sunyaev-Zel'dovich (SZ) effect, caused by the inverse Compton scattering of photons from the cosmic microwave background (CMB) by hot gas in clusters. The observable SZ effect signal (Y , the integrated Comptonisation parameter) does correlate well with cluster dynamical mass. The cluster mass can be estimated from measuring the one dimensional (1D) line-of-sight (LOS) velocity dispersion (σ_v) of galaxies in clusters, however, depending on the type of galaxies selected, such measurements may be subject to biases. We investigate this issue using simulated cluster and galaxy catalogues produced by the Millennium Gas Simulations Project. We aim to design an optimal observing strategy which is important for future dynamical mass measurements of Atacama Cosmology Telescope (ACT) clusters that aim to use the Southern African Large Telescope (SALT) for much larger studies of dynamical mass measurements (M_{500}).

We describe the methods used to make mock cluster catalogues by following the same procedure used in multi-object spectroscopic observations with the Robert Stobie Spectro-

graph. In our case we applied a different number of slits masks for targeting the galaxy clusters and investigate the impact it has on the recovered σ_v and estimated M_{500} . We do this for both an idealized case (100% redshift z completeness), and for a realistic case, where redshift completeness decreases for fainter objects. We calculate the velocity dispersion (σ_v) of each cluster at $z = 0.3$ using galaxies selected as members only, and then use galaxy cluster scaling relations derived from N-body/hydrodynamic simulations to estimate the cluster dynamical mass M_{500} . The recovered velocity dispersion is almost unbiased (1.5–2%) but with much bigger scatter (12–18%). We found that the bias of the estimated M_{500} for 100% z completeness is less than that for the realistic z incompleteness, which is as expected. For realistic redshift completeness, the bias in recovered M_{500} ranges from 11–30%.

The ultimate goal for this project is to determine how many masks we need to use per cluster, and how many clusters in total we need, to make a reasonable measurement of the $Y_{500}D_A^2 - \sigma_v$ relation, since the observing time on a queue-scheduled telescope such as SALT is quantized by how many masks are allocated to each cluster. Using a Markov Chain Monte Carlo (MCMC) method to fit the $Y_{500}D_A^2 - \sigma_v$ relation, we found that the recovered slope of the relation has less bias when using a large sample of clusters with poor quality σ_v measurements, as compared to a smaller sample of clusters with high quality σ_v measurements.

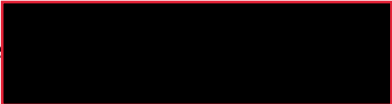
Preface and Declaration

The work described in this dissertation was carried out in the School of Mathematical Sciences, University of KwaZulu-Natal, Durban, from 25 February 2014 to June 2016, under the supervision of Dr Matt Hilton

These studies represent original work by the author and have not otherwise been submitted in any form for any degree or diploma to any tertiary institution. Where use has been made of the work of others it is duly acknowledged in the text.

Nhlakanipho Kwazi Mthembu

June 2016

Signature: : N.K Mthembu ----- Date: 14 Dec 2016 -----

Acknowledgments

It has been a great privilege to work on this project, which has very been challenging and exciting to work on and I feel very fortunate to have been involved in it.

In particular, I thank Matt Hilton my supervisor for his guidance, encouragement, advocacy, and patience, it has been a pleasure to work with him. The School of Mathematics, Statistics, and Computer Science is full of very supportive staff. I additionally thank the amazing members from Astrophysics & Cosmology Research Unit (ACRU) who provided me with quality mentorship during the course of my research to help me grow as a young researcher. I would also like to acknowledge the great financial support from the National Research Foundation and the University of KwaZulu-Natal.

Finally, I would like to thank my family and partner for their endless love and support. They made me feel free to pursue my interest in science and they continue to support my long journey ahead in Astronomy.

Contents

Abstract	ii
Preface and declaration	iii
Acknowledgments	iv
Contents	v
List of Tables	vii
List of Figures	viii
1 Introduction	1
1.1 Introduction to Cosmology	3
1.2 Galaxy Clusters	6
1.2.1 Clusters as Cosmological Probes	9
1.2.2 Cluster Cosmology	10
1.3 Observational Properties of Clusters	11
1.3.1 Optical Observation of Clusters	12
1.3.2 X-ray Observations of Clusters	14

1.3.3	Millimetre-Wavelength Observations	16
1.3.3.1	Cosmic Microwave Background	16
1.3.3.2	The Sunyaev-Zel'dovich (SZ) Effect	18
1.3.3.3	Sunyaev-Zel'dovich (SZ) Effect Observations	21
2	Cosmological Simulations of Galaxy Clusters	26
3	Mock SALT cluster observations and analysis	35
3.1	South African Large Telescope (SALT) Multi-Object Spectroscopy	36
3.2	Cluster Sample	38
3.3	Data Analysis and Results	42
3.3.1	Extraction of Simulated Galaxy and Cluster Catalogues from MGSs to mimic real Cluster Catalogues	43
3.3.2	Determining Galaxy Cluster Members	44
3.3.3	Recovered Velocity Dispersion	47
3.3.4	Dynamical Cluster Mass Estimates	48
4	SZ Scaling Relations	54
5	Conclusion	71
	Bibliography	72

List of Tables

4.1	The best-fit $Y_{500}D_A^2 - \sigma_v$ scaling relation parameters assuming 100% redshift z completeness (see text for more details).	63
4.2	The best-fit $Y_{500}D_A^2 - \sigma_v$ scaling relation parameters, assuming redshift z completeness as a function of magnitude as in Kirk et al. (2015) where we applied the SALT redshift z success rate (see text for more details).	64

List of Figures

1.1	Modern version of Hubble's plot	7
1.2	Illustration of sensitivity of the cluster mass function to the cosmological model	10
1.3	Image taken from Rosati et al. 2002 that shows the relation between ICM temperature, T , plotted against LOS velocity of a sample of galaxy clusters	17
1.4	Schematic diagram illustrating the SZ effect	19
1.5	Schematic representation that shows the distortion of the CMB due to the SZ effect	22
1.6	Plot illustrating the spectral distortion of the CMB due to the SZ effect . .	23
1.7	Scaling relation plot between dynamical mass (M_{200c}) vs. SZ signal (Y_{200c})	25
2.1	The image gives a visual impression of a simulated Universe	30
2.2	SZ effect images for a sample of galaxy clusters from the Millennium Gas Project	33
2.3	Scaling relations between the SZ flux, Y_{500} , and cluster total mass, M_{500} . .	34
3.1	Finder chart for an example SALT slit mask design	39
3.2	Redshift success rate as a function of magnitude (from Kirk et al. 2015) . .	40

3.3	The colour-magnitude diagram for one of the targeted galaxy clusters from the Millennium Gas Project	45
3.4	Graph of how well velocity dispersion is recovered from galaxies selected as cluster members	49
3.5	Cluster dynamical mass ($M_{500true}$) vs. velocity dispersion (σ_{1D}) as measured from the Millennium Gas Project	51
3.6	Graph showing how well cluster mass (M_{500}) is estimated using scaling relation	52
3.7	Graph showing how well cluster mass (M_{500c}) is estimated using scaling relation	53
4.1	The $Y_{500}D_A^2 - \sigma_{1D}$ relation for the Millennium Gas Project simulated clusters	55
4.2	The $Y_{500}D_A^2 - \sigma_v$ scaling relation for 100% z completeness when about 26 clusters were randomly selected initially	59
4.3	The $Y_{500}D_A^2 - \sigma_v$ scaling relation for realistic z completeness when about 26 clusters were randomly selected initially	60
4.4	The $Y_{500}D_A^2 - \sigma_v$ scaling relation for 100% z completeness when about 51 clusters were randomly selected initially	61
4.5	The $Y_{500}D_A^2 - \sigma_v$ scaling relation for realistic z completeness when about 51 clusters were randomly selected initially	62
4.6	The $Y_{500}D_A^2 - \sigma_v$ scaling relation for 100% z completeness when about 69 clusters were randomly selected initially	65
4.7	The $Y_{500}D_A^2 - \sigma_v$ scaling relation for realistic z completeness when about 69 clusters were randomly selected initially	66
4.8	The $Y_{500}D_A^2 - \sigma_v$ scaling relation for 100% z completeness when about 90 clusters were randomly selected initially	67
4.9	The $Y_{500}D_A^2 - \sigma_v$ scaling relation for realistic z completeness when about 90 clusters were randomly selected initially	68
4.10	Recovery of the true slope of the $Y_{500}D_A^2 - \sigma_v$ relation as a function of the sample size, for 100% redshift completeness	69

4.11 Recovery of the true slope of the $Y_{500}D_A^2 - \sigma_v$ relation as a function of the sample size, for realistic redshift completeness. 70

CHAPTER 1

Introduction

Galaxy clusters are the most massive gravitationally bound structures in the Universe, with the sizes of a few Mpc (a Mpc is about 3 million light years). On average clusters contain hundreds or thousands of galaxies, and most of their mass in the form of dark matter (DM), an unknown substance that makes up $\sim 23\%$ of the total mass-energy density of the Universe (Komatsu et al., 2011). The existence of DM is inferred indirectly, by its gravitational influence on galaxy clusters. Clusters are an excellent tool to study the history of the Universe and constrain cosmological parameters.

To probe cosmological parameters requires the knowledge of cluster mass, which is a quantity that is not directly observable, but can be predicted by numerical simulations of structure formation. Through observation, a number of proxies can be used to infer cluster mass. In our case we use the velocity dispersion of member galaxies to estimate the total dynamical cluster mass. However one cannot avoid picking up a fraction of foreground/background interlopers, i.e., galaxies that lie along the line-of-sight (LOS) and appear to be associated with the cluster. There are not gravitationally bound to the cluster

and their addition leads to a bias in the velocity dispersion based measurements used to estimate the total cluster mass (e.g., [Biviano et al., 2006](#); [Borgani et al., 1997](#); [Cen, 1997](#); [Lucy, 1983](#); [Mamon et al., 2010](#); [Wojtak et al., 2007](#)). This is the one of many reasons why we need to have well calibrated methods for cluster mass based measurement.

In this project, mock observations of galaxy clusters were produced, which closely mimic the constraints on target galaxy selection that affect real spectroscopic observations, and then their velocity dispersions were measured using techniques commonly applied to real data. We used the Millennium Gas Simulations (MGSs; [Kay et al., 2012](#), see Chapter 2) as the basis for the mock observations. We apply real observational methods that have been carried out with the South African Large Telescope (SALT; Buckley et al. 2006) when conducting Multi-Object Spectroscopy (MOS) of galaxy clusters with the Robert Stobie Spectrograph (RSS; Burgh et al. 2003). [Kirk et al. \(2015\)](#) did a follow-up study of the galaxy clusters that were recently detected with the Atacama Cosmology Telescope (ACT, [Swetz et al., 2011](#)) via the Sunyaev-Zel'dovich (SZ) effect. This is the inverse Compton scattering of photons from the cosmic microwave background (CMB) by hot gas in clusters ([Carlstrom et al., 2002](#)). The SZ-selected clusters targeted by SALT were those previously detected by the ACT team ([Hasselfield et al., 2013a](#); [Menanteau et al., 2013](#)).

In Chapter 1, we give a brief introduction about the motivation of the project, followed by an introduction to cosmology, galaxy clusters, observational properties of clusters and cluster scaling relations. In Chapter 2 we describe cosmological simulations of galaxy clusters and also the MGSs that we used for this project. In Chapter 3 we describe our data analysis and making the mock cluster observations. In Chapter 4 we talk about the SZ scaling relations and show the results of fitting the SZ signal–velocity dispersion relation. We present the conclusions of the thesis in Chapter 5.

Unless otherwise stated, throughout this thesis we adopt a flat Λ cold dark matter (Λ CDM) cosmology with present day parameters; $\Omega_m = 0.25$, $\Omega_\Lambda = 0.75$, a Hubble constant

of $H_0 = 73 \text{ km s}^{-1} \text{ Mpc}^{-1}$ and $\sigma_8 = 0.8$.

1.1 Introduction to Cosmology

Cosmology is the scientific study of the large scale properties of the Universe as a whole, bringing together ideas, and clarification about its birth. It aims to explain the origin and evolution of the entire contents of the Universe in order to have a deeper understanding of the physical processes that govern the formation of the large-scale structure. In the early days of cosmology, very little was known about this field of science, but in the modern era, there has been tremendous growth, provided by very powerful and sensitive instruments designed for astronomical observations.

The Universe is believed to have began with a very massive explosion called the Big Bang approximately 13.8 Gyr ago (see, [Planck Collaboration et al., 2015](#)). Right after the Big Bang it is thought that there was cosmic inflation, where there was an exponential expansion for approximately 10^{-37} s (e.g., see, [Roos, 2008](#)). After inflation the Universe carried on to expand while cooling down and allowing the formation of baryons. The process that manufactured the lightest elements in the early Universe is known as Big Bang nucleosynthesis.

The Universe today is full of structures of broad scales; the planets that orbit the stars, stars that make up galaxies, the galaxies which are gravitationally bound into clusters, and even clusters of galaxies that are also found within larger superclusters. In cosmology we seek to study all these vast range of structures as a whole. Cosmology deals with very huge scales, on which even galaxies are regarded to be very small. By our own human standards, the Universe is very old but on a cosmological point of view the present Universe is not indefinitely old.

Our modern theory of cosmology is based on the assumption that the Universe is ho-

mogeneous and isotropic on large scales. Homogeneity is the statement that the Universe looks the same at each point, while isotropy states that the Universe looks the same in all directions. We call this the cosmological principle. It is important to stress that the cosmological principle is not precise but rather a postulation, that holds better and better the larger the length of the scale we look at. For instance, our own galaxy, the Milky Way, is not a special place in the Universe, but is just one amongst billions of other galaxies that are scattered across the universe.

The cosmological principle is not very good on scales of individual galaxies, but once we take very large regions, say, containing about a million galaxies, we anticipate the Universe to look the same in all directions and also look the same at each point. The cosmological principle is supported by observations of the expanding universe, from which it follows that everyone at any one instant in time must see the same rate of expansion. The cosmological principle is therefore a property of the global Universe, breaking down if one looks at the local occurrence phenomena. It is also the basis of the "Hot Big Bang" model for cosmology, which is currently the best approximation we have to explain the birth of our Universe and its current state.

In the 1920's Edwin P. Hubble measured the recession velocities of about 18 spiral galaxies with known distances and he found that all of the velocities increased linearly with distance ([Hubble, 1929](#)),

$$v = H_0 r, \tag{1.1}$$

where H_0 (now called Hubble's constant) is the constant of proportionality between recession speed v and distance r . Hubble was the first to establish the correct law of expansion of the Universe. He found correlation between the distance to a galaxy and its recessional velocity as determined by the redshift z . The wavelength of the light emitted from far away galaxies which is moving along the line of sight towards an observer on Earth is stretched along with the expansion of the Universe and the observed galaxy light from Earth has a

redshift z , given by

$$z \equiv \frac{\lambda_0 - \lambda_e}{\lambda_0}, \quad (1.2)$$

where λ_0 is the rest-frame wavelength and λ_e is the wavelength of at the time of emission. The redshift of distant galaxies can be measured from looking at a galaxy spectrum. When a galaxy has a redshift of $z < 0$, we say it is blueshifted. This happens to galaxies coming towards our own, but a vast majority of galaxies are redshifted (i.e., $z > 0$). This increase of the velocity of recession according to Hubble is directly proportional to the galaxy's distance.

Figure 1.1 shows a modern measurement of the Hubble law by the HST Key Project [Freedman et al. \(2001\)](#). The present day values of cosmological parameters, like H_0 , are always subscripted by “0”, which refers to the present epoch ($z = 0$). The value of the Hubble parameter changes with redshift.

One of the most astonishing things about relativistic cosmology is that the Universe has not existed forever. There is a finite time-frame that separates mankind from the extremes of the energy and density in which the expanding Universe started off from. One of the biggest questions in cosmology is: How old is the Universe? The approximate age of the universe is given by the Hubble time t_H , which is the inverse of the Hubble constant,

$$t_H \equiv \frac{1}{H_0} = 9.78 \times 10^9 h^{-1} yr = 3.09 \times 10^{17} h^{-1} s, \quad (1.3)$$

where h is the dimensionless parameter scale factor for the Hubble expansion rate that is said be $h = 0.72 \pm 0.02$ (see, [Freedman et al., 2001](#)).

In the Big Bang model, the Universe is expanding, from an initially hot and dense state and has been expanding since its birth (see., [Mo et al., 2010](#), for more details). The expansion is still going on even today, and at an accelerating rate, as discovered from observations of Type Ia supernovae([Perlmutter et al., 1999](#); [Riess et al., 1998](#)). The discovery of cosmic acceleration was a major milestone for modern cosmology. It was the first evidence that

supported the existence of dark energy (DE), which is responsible for expansion of Universe and causes it to happen at an accelerated rate. Even after the discovery of an accelerating expansion of the Universe, the physical origin of DE still remains a deep mystery. DE is a theoretical form of energy that exerts a negative, repulsive pressure, postulated to act in opposition to gravity, and it makes up $\sim 73\%$ of the total mass-energy density of the Universe (see, [Komatsu et al., 2011](#); [Yoo & Watanabe, 2012](#)).

One of the most fundamental problems in cosmology is to compile a census of the contents of the Universe. In the sections to follow we talk more about methods used to learn more about gas, radiation, DM and galaxies that together make up contents of the observed Universe. One way to measure the energy density of the universe in terms of both matter and dark energy is to study the properties of galaxy clusters.

1.2 Galaxy Clusters

The observable Universe is made up of $\sim 4.6\%$ ([Komatsu et al., 2011](#)) baryonic material. There over 100 billion galaxies, and they can be classified into a different range of categories depending on their shape and size, there are: elliptical, spiral, irregular and dwarf galaxies. There are also many sub-categories within the above mentioned classification (see, [van den Bergh, 1976](#), for a more detailed classification). Most galaxies have a total mass $\sim 10^7 - 10^{12} M_{\odot}$, and their size range from few kpc to over 100 kpc in diameter. Galaxies are not randomly distributed in space but normally reside in groups or in much larger agglomerations called clusters. The smaller aggregates of galaxies are called a group of galaxies rather than cluster of galaxies, normally consisting of 50 or fewer gravitationally-bound member galaxies. Our own galaxy The Milky Way is a member of galaxies known as The Local Group, including the larger spiral galaxy Andromeda (M31) and several smaller satellites, which include the Large and Small Magellenic Clouds. The Local Group consists of ~ 30 members.

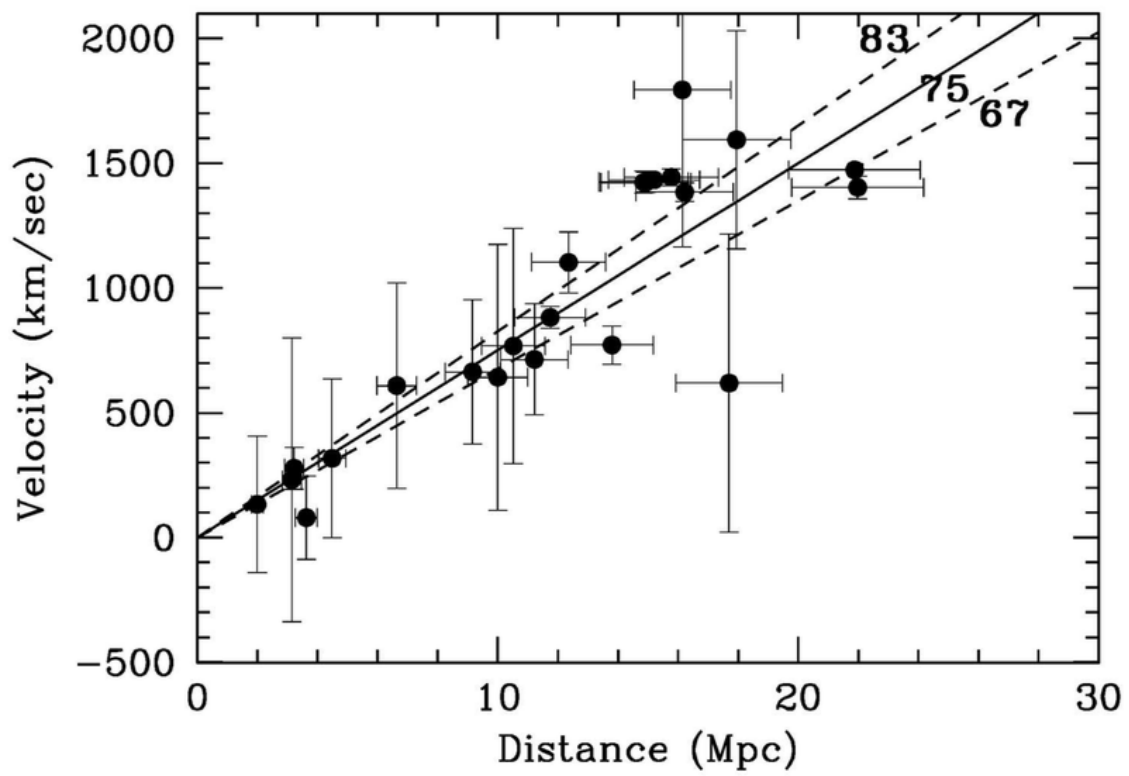


Figure 1.1: Modern version of Hubble's plot by (Freedman et al., 2001, from HST Key Project) using Cepheid variable's of stars as standard candles. This plot shows the relation between recession velocity and the distance.

Galaxies clusters consist of ~ 100 – 1000 s of bright galaxy members that are bound together by gravity. Galaxy clusters normally fall into the classification referred to as regular galaxy clusters which are spherically shaped, usually rich, meaning they have ~ 1000 's of galaxy members. They have large galaxies at the centre, and most galaxies found in regular clusters are either elliptical or lenticular. An example of a regular cluster is the Coma cluster. A typical mass of cluster ranges from 10^{14} – 10^{15} M_{\odot} , with most of the mass being; about over 80% DM, $\sim 15\%$ of hot gas, and less than 5% of luminous matter like stars. The heated gas found between galaxies is called the intracluster medium (ICM), which has a temperature peaking at 2–15 keV but varies with the total mass of the cluster. The ICM provides us with a good environment for testing our understanding galaxy cluster formation (see, [Padmanabhan et al., 1993](#), for more details on clusters and structure formation).

Most of the visible mass in galaxies is mainly from stars but the fundamental theories of cosmology and observational evidence suggest that DM is the most dominant component in galaxy clusters. This form of matter is neither stellar nor gaseous, which makes the nature of DM elusive, and further complicates the use of clusters as cosmological probes. DM does not interact with light; it is collisionless and dissipationless, unlike gas (see [Bertone, 2010](#), for more details on the properties of DM). To date, no one has ever directly detected signals from DM. A lot of improvements are being made through cosmological numerical simulations with DM particles and observational experiments to enhance our knowledge and give us a deep overview understanding of the unknown physical processes of the Universe.

The characteristics of galaxies makes them convenient to use for tracing the history of the Universe. By studying them and being able to have well-calibrated methods to measure their mass more accurately may give us insight into how structure has grown in our universe.

1.2.1 Clusters as Cosmological Probes

The Universe can be described in terms of the cosmic web structure from very large structures called superclusters, to clusters of galaxies and to smaller scales that contain galaxy groups. The cosmic web also consists of areas with nearly empty voids, this means that the growth structure of the Universe and matter distribution follows a hierarchical pattern. Clusters of galaxies are considered one of the most important cosmological probes. In order to extract information from galaxy clusters we must be able to classify them distinctively from other objects in the Universe and also understand their formation process at a given epoch. With a considerate analysis of galaxy cluster properties at different structure levels this can help us understand in more detail the history of the growth of structure in the Universe. Due to the fact that clusters contain a lot of information about their own evolution, they serve as the natural laboratories in which to study the formation history of the universe.

Previous studies of galaxy clusters have contributed a vast wealth of information which has helped to improve measurements of the standard cosmological model parameters. Clusters are a sensitive probe for cosmology (e.g., see, [Vikhlinin et al., 2009](#)), as shown by [Figure 1.2](#), which illustrates the sensitivity of the cluster mass function to the underlying cosmological model. The panel on the left has $\Omega_\Lambda = 0.75$ and the panel on the right has $\Omega_\Lambda = 0$. The observations (points with error bars) are not a good match to the model with $\Omega_\Lambda = 0$, so from this illustration of [Figure 1.2](#), clusters can be used to constrain Ω_Λ and other cosmological parameters.

Observational data of galaxy clusters have been used to provide useful measurements for constraining cosmological parameters (e.g., [Allen et al., 2011](#)). In spite of all the huge amounts of rich data clusters can provide, probing strong constraints from cluster surveys is still a non-trivial problem due to the complexity of estimating accurate cluster masses. More work still needs to be done with regards to understanding DM and DE since they

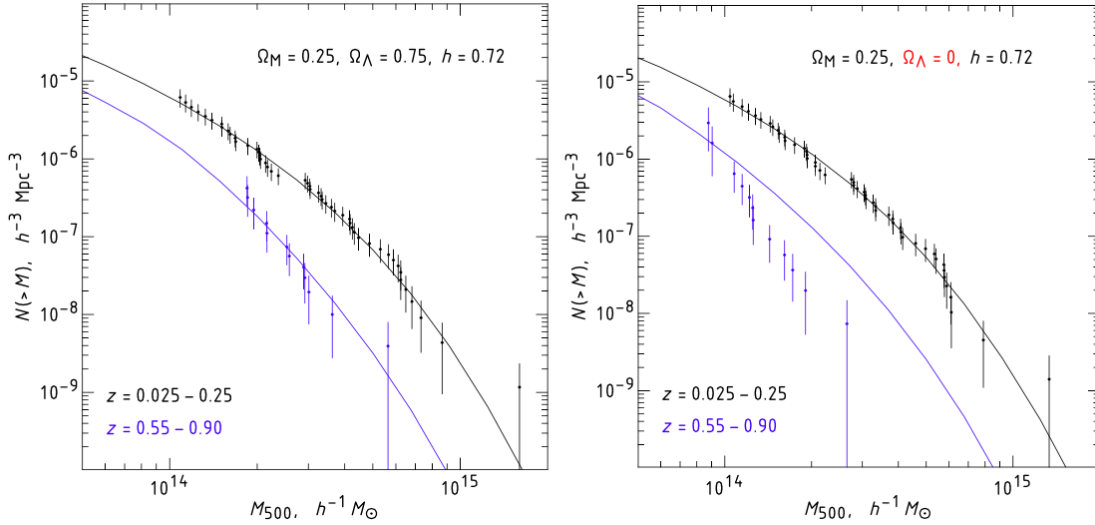


Figure 1.2: Illustration of sensitivity of the cluster mass function to the cosmological model, the solid lines show the mass function models (weighted with the survey volume as a function of cluster mass and redshift z). The panel on the left has $\Omega_\Lambda = 0.75$ and the panel on the right has $\Omega_\Lambda = 0$. (Image credit (Vikhlinin et al., 2009)).

both dominate the Universe and no one has ever directly observed signals of both. This is because almost if not all of the information we have about galaxy clusters comes to us from photons: optical photons from stars, radio photons from neutral hydrogen gas, X-ray photons from ionized gas and so forth (e.g., Sarazin et al., 1988).

1.2.2 Cluster Cosmology

Clusters of galaxies correspond to the regions of the resulting large-scale structure. The spatial distribution and number density of clusters carries the imprint of the process of structure formation and, as a consequence, these properties are sensitive to the underlying cosmological parameters. The number density of galaxy clusters as a function of their mass M and redshift z , $N(M, z)$, is strongly dependent on the cosmological parameters; Ω_Λ the DE density of the Λ CDM Universe, Ω_m the pressureless matter density of the Universe, and σ_8 the amplitude of density fluctuations on scales of 8 Mpc.

In order to use clusters to constrain cosmological parameters, we need to know their masses as precisely as possible. Cluster mass can be determined in several ways, e.g., by measuring the gravitational lensing distortion of the images of background galaxies by means of weak and strong lensing (see, [Hoekstra et al., 2013](#)) which is said to be a direct way, or by assuming the condition of viral equilibrium, through measurements of the velocity dispersion of the cluster of galaxies. These methods of mass measurements can only be applied to clusters for which high-quality data are available, and obtaining individual mass measurements for a large number of systems is observationally exorbitant. Cluster mass can also be inferred from other more easily measured observables, using scaling relations to relate these measurements to the cluster mass (e.g., [Kravtsov & Borgani, 2012](#)). Examples of these include: the velocity dispersion of member galaxies (e.g., [Biviano et al., 2006](#); [Saro et al., 2013](#)), the total thermal content of the intracluster plasma measure from SZ or X-ray (e.g., [Arnaud et al., 2010](#); [Kay et al., 2012](#); [Williamson et al., 2011](#)) observations, and the optical luminosity traced by the galaxy population (e.g., [Popesso et al., 2007](#)).

1.3 Observational Properties of Clusters

Observational studies of galaxy clusters have now developed into a broad, multi-faceted and multi-wavelength field. Over the past centuries astronomers have had to rely on the limited part of the spectrum in order to study the Universe but, with the advancement of technology, new modern ground based and space telescopes have allowed the exploitation of the full electromagnetic spectrum for astronomical measurements. There are now advanced telescopes capable of making observations at radio waves, microwaves, infrared light (IR), visible light (VI), ultraviolet light (UV), X-rays and gamma rays, which all correspond to light waves of different (in this case increasing) frequency (see, [Liddle, 2010](#)).

In Section [1.3](#) we outline how clusters are observed at X-ray, optical, and millimetre

wavelengths. We briefly explain some of their observational properties and the associated physical processes, which allow us to probe their dynamics at different redshifts. We also describe how these observational quantities can be related to cluster mass.

1.3.1 Optical Observation of Clusters

The identification of galaxy clusters by optical telescopes has been going on for quite a long time, and in the late 18th century Charles Messier and William Herschel had both discovered traces of galaxies in the constellations of Virgo and Coma. Large area cluster searches began with the pioneering photographic surveys by [Abell \(1958\)](#), Zwicky et al. (1968) and Sackett (1985). A great comprehensive advancement in the systematic study of the properties of clusters occurred when Abell compiled an extensive, statistically complete catalogue of rich clusters of galaxies ([Abell, 1958](#)) by looking for projected galaxy overdensities through visual inspection of photographic plates. Abell’s catalogues contain most known nearby galaxy clusters and are the foundation from which much of our modern understanding of clusters have grown.

Many improvements have been made to optical cluster identification methods, building on Abell’s approach (e.g., Dalton et al. 1997, Lumsden et al. 1992, Postman et al. 1996). The number of optically discovered clusters has been increasing over the past decades as the observing instrumentation power has been improving (see Biviano, 2000, for review of history). The colour of galaxies can help with identifying clusters, because cluster galaxies are notably redder than others at the same redshift, due to a lack of ongoing star formation. This places cluster members on a “red sequence” in a plot of galaxy colour versus magnitude (e.g., [Rykoff et al., 2014](#)).

The total optical luminosity of a cluster is itself an indirect measurement of a cluster’s mass. The luminosity function describes the distribution of galaxies in a cluster as a

function of luminosity. There are several functions that could be used for fitting the luminosity function and nowadays astronomers use the [Schechter \(1976\)](#) function

$$\phi(L)dL = \phi^*(L/L^*)^\alpha \exp(-L/L^*)d(L/L^*), \quad (1.4)$$

where $\phi(L)dL$ is the number density of galaxies with luminosities between L and $L + dL$, where L^* is a characteristic luminosity cutoff, α is the power-law slope at the faint-end, and ϕ^* is the normalisation (galaxies/Mpc³). It is often convenient to rewrite the Schechter function in terms of magnitudes, rather than luminosities. In this case the Schechter function becomes

$$\phi(M)dM = (0.4 \ln 10) \times \phi^* \times 10^{0.4(\alpha+1)(M^*-M)} \times \exp(-10^{0.4(M^*-M)})dM. \quad (1.5)$$

When conducting optical observations, it not possible to measure the luminosity of every galaxy in a cluster, especially at high redshift, where only the brightest galaxies can be observed. Since the luminosity distribution function of cluster galaxies is very much uniform from cluster to cluster, observing the high-luminosity peak of that distribution allows one to standardise the overall galaxy luminosity function for the cluster. The standardisation of the overall galaxy luminosity finally allows one to make estimates for both the cluster's total optical luminosity and its mass (from, [Voit, 2005](#)).

Optical observations also allow astronomers to perform measurements of orbital velocities of galaxies in clusters. As mentioned in the previous sections, galaxy clusters are the most massive gravitationally bound systems, and are believed to have undergone some sort of dynamical relaxation from irregular to regular clusters, with regular clusters being more relaxed than irregular clusters ([Voit, 2005](#)). The nature of this distribution can be studied by acquiring the radial velocities v_r (which is the component of the galaxy velocity along the line of sight) of the optically confirmed cluster members. The radial velocities v_r of individual galaxies are expected to be distributed around the mean radial velocity of galaxies in a cluster, which makes the velocity distribution of a relaxed cluster's galaxies to be gaussian in velocity space. The most conventional way to represent this distribution

is in terms of dispersion

$$\sigma_{1D} = \langle (v_r - \langle v_r \rangle)^2 \rangle^{1/2}, \quad (1.6)$$

where σ_{1D} is the one-dimensional (1D) velocity dispersion for the cluster. The first ever measurement of the velocity dispersion for a cluster was made by Zwicky (1933, 1937) for the Coma cluster where it was found to be $\sigma_{1D} \sim 700 \text{ km s}^{-1}$, although, because of the presence of background galaxies, it is not possible to state with absolute confidence that any given galaxy belongs to a given cluster. Thus, one cannot give an exact count of the number of galaxies in a cluster so the accuracy of the σ_{1D} relies on the method applied to identify the number of member galaxies with measured velocity and eliminating non-members such as interlopers that reside along the LOS but are not part of the cluster.

1.3.2 X-ray Observations of Clusters

The Earth's atmosphere is opaque to X-ray wavelengths of light, and so observations of celestial objects that emit X-ray photons had to be carried out from space. M87 in the Virgo cluster was the first extragalactic object to be detected as an X-ray source by (Bradt et al., 1967; Byram et al., 1966). Because observations of X-ray astronomy had to wait for more space based satellites to be developed and launched into space, progress in X-ray astronomy was slow, but in the early 1970s, the study of X-ray clusters started to accelerate after the launch of the Uhuru X-ray satellite (see, Forman et al., 1978). Uhuru also allowed more extended observational analysis to be done on individual X-ray sources as well as a complete all sky survey of the X-ray sources.

X-ray observations have allowed the properties of clusters to be studied, in particular the intracluster medium (ICM). The ICM is a super heated plasma that is present at the center of a galaxy cluster, and mostly emits X-ray radiation by the bremsstrahlung process. X-ray observations of numerous clusters of galaxies show that the radiation is sharply peaked around the central brightest galaxy, and the brightness of the X-rays tells us about

the density of the gas. By observing the hot diffused ICM and assuming the gas to be in hydrostatic equilibrium within the cluster gravitational potential well, mass estimates can be inferred from these X-rays observations (e.g., [Sarazin et al., 1988](#)) but this needs very precise measurement of the gas density and temperature. Satellites like Chandra and XMM-Newton are capable of measuring these quantities to high precision, but this has mostly been done for low redshift clusters. At high redshift, only a small number of clusters have hydrostatic mass estimates, due to the long observation times needed to measure the temperature profiles of such clusters.

One of the set backs of the hydrostatic equilibrium assumption, is that it only applies to clusters that are dynamically relaxed. If its not possible to estimate mass this way there are other methods such as scaling relations, whereby X-ray cluster observables such as luminosity, temperature or LOS velocity dispersion could be used to infer the mass. The average X-ray temperature is one of the most widely used cluster mass indicators (see, [Vikhlinin et al., 2008](#)), the $M - T$ relation expected in self-similar theory is given by,

$$M \propto T^{3/2} E(z)^{-1} \quad (1.7)$$

where,

$$E(z) \equiv H(z)/H_0. \quad (1.8)$$

where T is the ICM temperature (which can be measured from X-ray observations) and M the cluster mass. Equation 1.7 shows how cluster quantities, such as T , are directly related to cluster mass. The relation arises in the self-similar model simply because the ICM T is expected to scale with the depth of gravitational potential $T \propto M/R$ and mass and radius R are related as $R \propto M^{1/3}$, ([Borgani et al., 2004](#); [Evrard et al., 1996](#); [Mathiesen & Evrard, 2001](#)). X-ray observations of clusters allow us to probe the physics of the hot, diffuse ICM, which offers a completely different tracer to measure the total gravitating cluster mass (e.g., [Rosati et al., 2002](#)). Figure 1.3 shows scaling relations for distant clusters in the X-ray band. The plot on the left shows the relation between T and line of sight velocity dispersion, while the plot on the right shows the relation between X-ray luminosity and mass. The

correlation shown in Figure 1.3 between the cluster quantities indicates that the picture of clusters as relaxed structures in which both gas and galaxies feel the same dynamics is a reasonable representation (from, [Rosati et al., 2002](#)). The presence of scatter and outliers indicates there are more complex physical dynamics taking place. This suggest that more improvement needs to be done in order to improve measurements of scaling relations for galaxy clusters.

1.3.3 Millimetre-Wavelength Observations

1.3.3.1 Cosmic Microwave Background

The Cosmic Microwave Background (CMB) was discovered by [Penzias & Wilson \(1965\)](#), who found that the CMB radiation is present in all directions with almost equal intensity, although it was originally predicted in 1946 by [Gamow \(1946\)](#) as a result of the hot, dense early universe.

The origins of the CMB lie in the early hot phase of the expansion of the Universe, so the discovery of the CMB was a breakthrough for the Big-Bang theory prediction. It effectively sounded the death knell for the steady-state model of the universe, which at one point had many adherents, due to the appeal of a universe that does not change with time (see, [Liddle, 2010](#))

The CMB allows us to trace back the physical history of the universe using the fossilised heat from the Big Bang, which has now cooled due to the expansion of the universe. The unique properties of the CMB make it a very good probe of cosmology. By observing the CMB radiation and mapping its spectrum across the sky, we can gain insights into galaxy clusters, and in turn our understanding of cosmology.

The frequency spectrum of the CMB radiation was measured to high accuracy by the

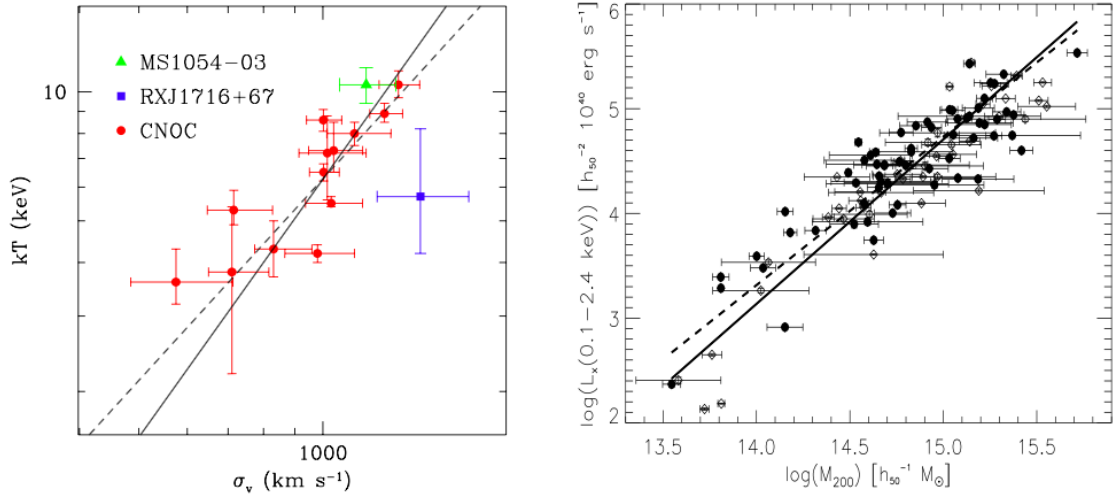


Figure 1.3: Image taken from Rosati et al. 2002. The left plot shows the relation between ICM temperature, T , plotted against LOS velocity dispersion, σ_v , of a galaxy clusters. σ_v was taken from Carlberg et al. (1997a) for CNOC clusters and from Girardi & Mezzetti (2001) for MS1054-03 and RXJ1716+67. Temperatures T are taken from Lewis et al. (1999) for CNOC clusters, from Jeltema et al. (2001) for MS1054-03 and from Gioia et al. (1999) for RXJ1716+67. The solid line shows the relation $k_B T = \mu m_p \sigma_v^2$, and the dashed line is the best-fit to the low- z $T - \sigma_v$ relation from Wu et al. (1999). The right plot shows the low- z relation between X-ray luminosity and the mass contained within the radius encompassing an average density $200\rho_c$ (from Reiprich & Bohringer 2002). The two lines are the best log-log linear fit to two different data sets indicated with filled and open circles

Cosmic Background Explorer (COBE) satellite (Boggess et al., 1992), which conducted a full-sky survey. COBE found that the spectrum of the CMB is indeed thermal, with a measured perfect body spectrum at temperature of about $T_{CMB} \approx 2.726$ K (Fixsen et al., 1996), and the intensity of the radiation field is almost completely isotropic (the same in all directions). The specific intensity of the radiation is therefore close to

$$I_\nu = \frac{2h\nu^3}{c^3} (e^{h\nu/k_B T_{CMB}} - 1)^{-1} \quad (1.9)$$

which correlates well with the maximum brightness $I_{max} \sim 3.7 \times 10^{-18}$ W m⁻² Hz⁻¹ sr⁻¹ at $\nu_{max} \sim 160$ GHz, a photon density $n_\gamma \sim 4 \times 10^8$ photons m⁻³, and an energy density $u_\gamma \sim 4 \times 10^{-14}$ J m⁻³, which can be represented as a mass density $\rho_\gamma \sim 5 \times 10^{-31}$ kg m⁻³, and is substantially smaller than the critical density

$$\rho_{crit} = \frac{H_0^2}{8\pi G} = 1.88 \times 10^{-26} h_{100}^{-2} \text{ kg m}^{-3} \quad (1.10)$$

required to close the Universe. In the above equation, h is Planck's constant, $h_{100} = H_0/100$ km s⁻¹ Mpc⁻¹ is a dimensionless estimation rate of the Hubble constant, H_0 , G is the gravitational constant, c is the speed of light, ν is the frequency, and k_B is the Boltzmann constant.

1.3.3.2 The Sunyaev-Zel'dovich (SZ) Effect

The hot gas that X-ray observations uncover from galaxy clusters may also be discovered in several other ways besides from thermal bremsstrahlung radiation. The photons that pass into and out of the cluster undergo what is known as inverse Compton scattering from colliding with excited high energy free electrons in the hot ($T > 10^7$ K) ICM (gas) which triggers a small fraction of the photons to become up scattered to higher energies, and this creates a small distortion in the CMB temperature. Figure 1.4, shows a cartoon version of this effect. This effect is now known as the Sunyaev-Zel'dovich (SZ) effect (Sunyaev & Zeldovich, 1972) which is a very powerful tool now being used for detecting, and for

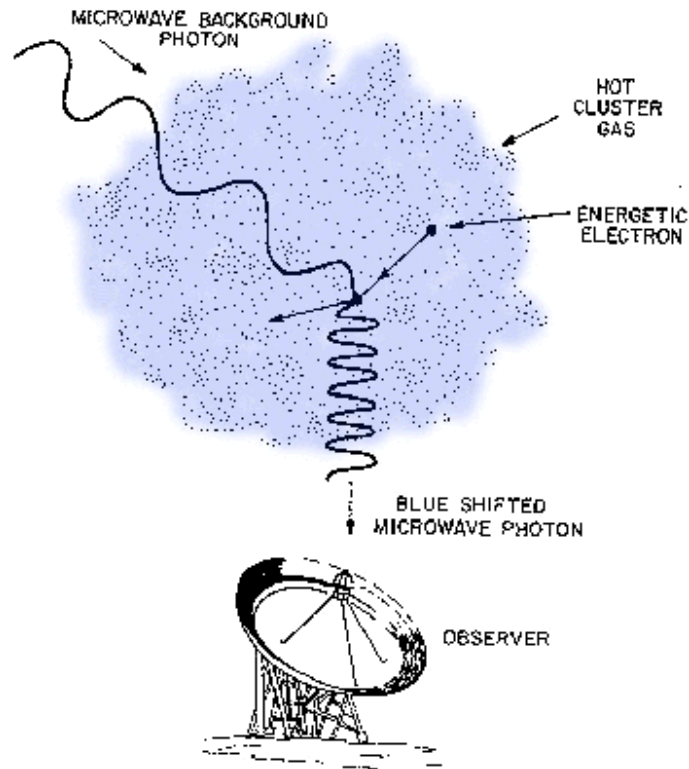


Figure 1.4: Schematic diagram of SZ effect, this phenomenon arises when low-energy photons of the CMB pass through the hot ionised intracluster gas in a rich cluster of galaxies. The picture shows the scattering of CMB photons by rapidly moving electrons in the hot gas in the cluster. Clusters are revealed by measuring the distortion of the CMB spectrum owing to the hot ICM. It is one of the most powerful methods to find distant clusters and does not depend on redshift z and provides reliable estimate of cluster masses. (Adapted from L. Van Speybroeck)

discovering new clusters (see, [Carlstrom et al., 2002](#); [Marriage et al., 2011](#); [Planck Collaboration et al., 2014](#); [Vanderlinde et al., 2010](#), for more details on SZ effect clusters) at high z .

The effect that is observed is proportional to the number density of electrons, n_e , the thickness of the cluster along the line of sight, and the electron temperature, T_e . The parameter that combines these factors is called the SZ y parameter. The y parameter is measured along the LOS towards massive clusters.

Something of relevant interest about the SZ effect is that it conserves photons. If there is no interaction, photons cannot be created or absorbed, only scattered, which redistributes their energies. To examine the SZ effect, we derive the transport equations that govern the whole effect of the inverse Compton scattering on the photon energy distribution. The observed spectral distortion in the CMB intensity is given by,

$$\Delta I(x) = 2 \frac{(k_B T_{CMB})^3}{(hc)^2} y g(x), \quad (1.11)$$

expressed in units of specific intensity, where

$$\Delta I(x) = I(x) - I_0(x), \quad (1.12)$$

$I(x)$ is the up-scattered CMB spectrum in the direction of the cluster and $I_0(x)$ is the unscattered CMB spectrum in the direction of the sky area close to the cluster, T_{CMB} is the incident CMB temperature,

$$x = h\nu/k_B T_{CMB}, \quad (1.13)$$

and

$$g(x) = x^4 e^x (x(e^x + 1)/(e^x - 1) - 4)/(e^x - 1)^2. \quad (1.14)$$

The inverse Compton scattering increases the frequency of a scattered photon by an average amount $\Delta\bar{\nu}$ of

$$\frac{\Delta\bar{\nu}}{\nu} = 4 \frac{kT_e}{m_e c^2} \quad (1.15)$$

where T_e is the temperature of the electron gas, m_e is the electron mass and c the speed of light. The resulting distortion of the CMB spectrum is shown in [Figure 1.5](#) and [1.6](#).

Figure 1.5 shows the SZ effect of the CMB spectral distortion for a fictional cluster that is over 1000 times more massive than a typical cluster to illustrate the small effect (e.g., Carlstrom et al., 2002).

The SZ observable Y parameter is

$$Y = \int y \, d\Omega, \quad (1.16)$$

where the integral is performed over the solid angle subtended by the cluster. The Comptonization y parameter is defined by the thermal structure of the ICM:

$$y = \frac{\sigma_T k_B}{m_e c^2} \int P_e dl, \quad (1.17)$$

in terms of the pressure where $P_e = n_e T_e$ which is contributed by the electronic population, n_e and T_e are the density and temperature of the free electrons respectively and dl is the differential along the line of sight, and σ_T is the Thomson cross section. For a gas that is in hydrostatic equilibrium and is within the cluster's gravitational potential well, the electron temperature T_e can be determined by

$$k_B T_e \approx \frac{GMm_p}{2R_{eff}}, \quad (1.18)$$

where M is the cluster mass, G is the gravitational constant and m_p is the proton mass. At this temperature, thermal emission from the gas appears in the X-ray part of the spectrum, and is composed of thermal bremsstrahlung and line radiation (see, Birkinshaw, 1999).

Figure 1.6 shows that the SZ effect has a distinct frequency dependence such that, in the direction of a massive cluster, the temperature of the sky increases at frequencies larger than 218 GHz while below this frequency the temperature decreases.

1.3.3.3 Sunyaev-Zel'dovich (SZ) Effect Observations

The SZ effect is a powerful method for discovering new clusters of galaxies. Early measurements of the SZ effect were performed with targeted observations of known clusters. These

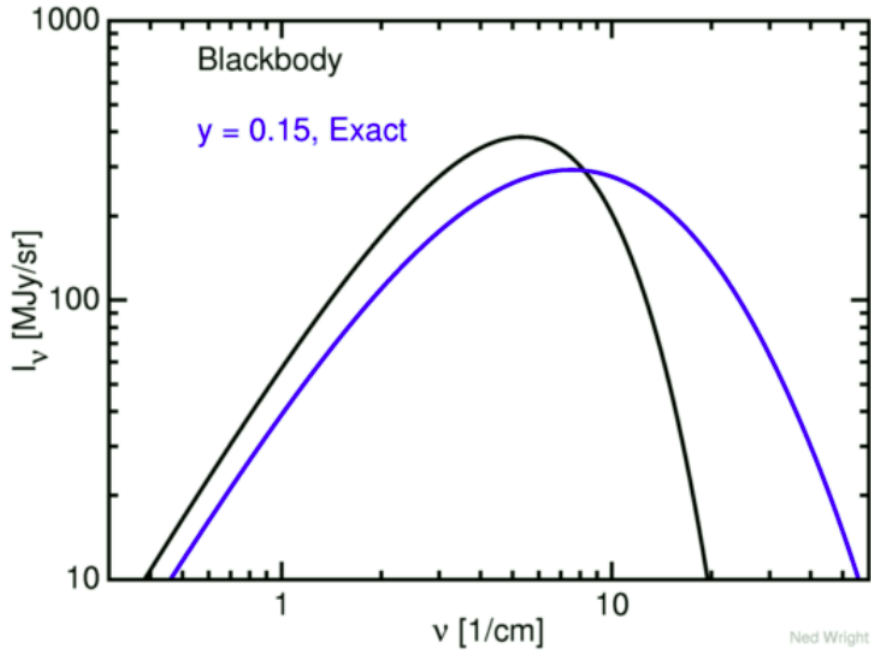


Figure 1.5: The diagram shows Cosmic Microwave Background (CMB) spectrum, for undistorted shown by the black solid-line and the distorted CMB due to the Sunyaev-Zel'dovich (SZ) effect is shown by the blue solid-line, the plots where done on a log-log scale. The diagram shows photons from CMB that are scattered to higher frequencies by colliding with the high energy electrons in the hot intracluster gas. For frequencies less than the peak frequency, more photons are scattered out of a frequency interval than into it, so the intensity at that frequency decreases. Similarly, for frequencies greater than the peak frequency, fewer photons are scattered out of a frequency interval than into it, so the intensity at that frequency increases. The net results is a shift of the CMB spectrum to higher frequencies. Figure from Ned Wright (www.astro.ucla.edu/wright/SZ-spectrum.html)

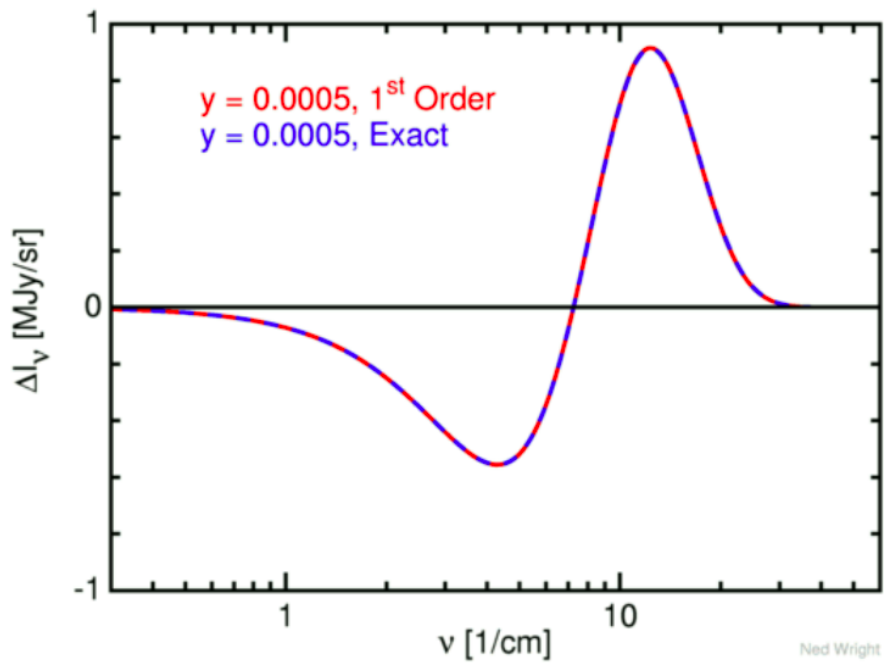


Figure 1.6: Spectral distortion of the cosmic microwave background (CMB) spectrum radiation due to the thermal Suyae-Zel'dovich (SZ) effect on a log-log scale for a realistic massive cluster (a Compton y parameter of $y = 10^{-4}$). The SZ effect causes a decrease in the CMB intensity at frequencies ≤ 218 GHz and an increase at higher frequencies (Carlstrom et al., 2002). Figure from Ned Wright (www.astro.ucla.edu/wright/SZ-spectrum.html)

studies revealed the power of the SZ effect, for studying gas physics and the inner structures of clusters (Benson et al., 2004; Grego et al., 2001). The SZ signal does not diminish due to luminosity distance: it is nearly redshift independent, and so SZ surveys can detect all clusters in the universe above a mass limit set by the survey noise level (e.g., Birkinshaw, 1999; Carlstrom et al., 2002). The first blind detections of galaxy clusters through their SZ effect were reported by Staniszewski et al. (2009). Over the past few years there has been tremendous growth in surveys carried out to detect clusters via SZ effect. The largest SZ cluster catalogue has been provided by the all sky survey conducted by the Planck Collaboration (Planck Collaboration et al., 2014) showing results of an all-sky Planck catalogue of cluster candidates derived from SZ effect detections. The South Pole Telescope (SPT; Carlstrom et al., 2011; Padin et al., 2008) also conducted a 2500 square degree SZ cluster survey. The Atacama Cosmology Telescope (ACT Swetz et al., 2011) has also surveyed 504 square degrees on the celestial equator (Hasselfield et al., 2013a; Menanteau et al., 2013) in order to search for SZ clusters. ACT is a 6m off-axis Gregorian telescope located at an altitude of 5200 m in the Atacama Desert in northern Chile, it was designed to measure small-scale anisotropies in the CMB, and observe the sky in three frequency bands (centred at 148, 218, and 277 GHz) simultaneously with arcminute resolution.

Previous studies have shown that the observable SZ signal (Y , the integrated Comptonisation parameter) does correlate well with cluster dynamical mass. Figure 1.7 shows the scaling relation between dynamical mass (M_{200c} , measured from the velocity dispersion of galaxies in clusters) and SZ signal (Y_{200c}), measured from ACT data (Sifón et al., 2013). The ACT data were fitted using a power-law of the form

$$\frac{M_{200c}}{h^{-1}M_{\odot}} = 10^A \left(\frac{Y_{200c} D_A(z)^2 E(z)^{-2/3}}{Y_{pivot}} \right)^B. \quad (1.19)$$

The solid blue line in Figure 1.7 shows the best-fit line of Equation 1.19, with $Y_{pivot} = 5 \times 10^{-5} h^{-2} \text{ Mpc}^2$, and the gray shaded region shows the 1σ uncertainty. Other measurements shown in Figure 1.7 are from either observations or simulations, as indicated by the coloured lines.

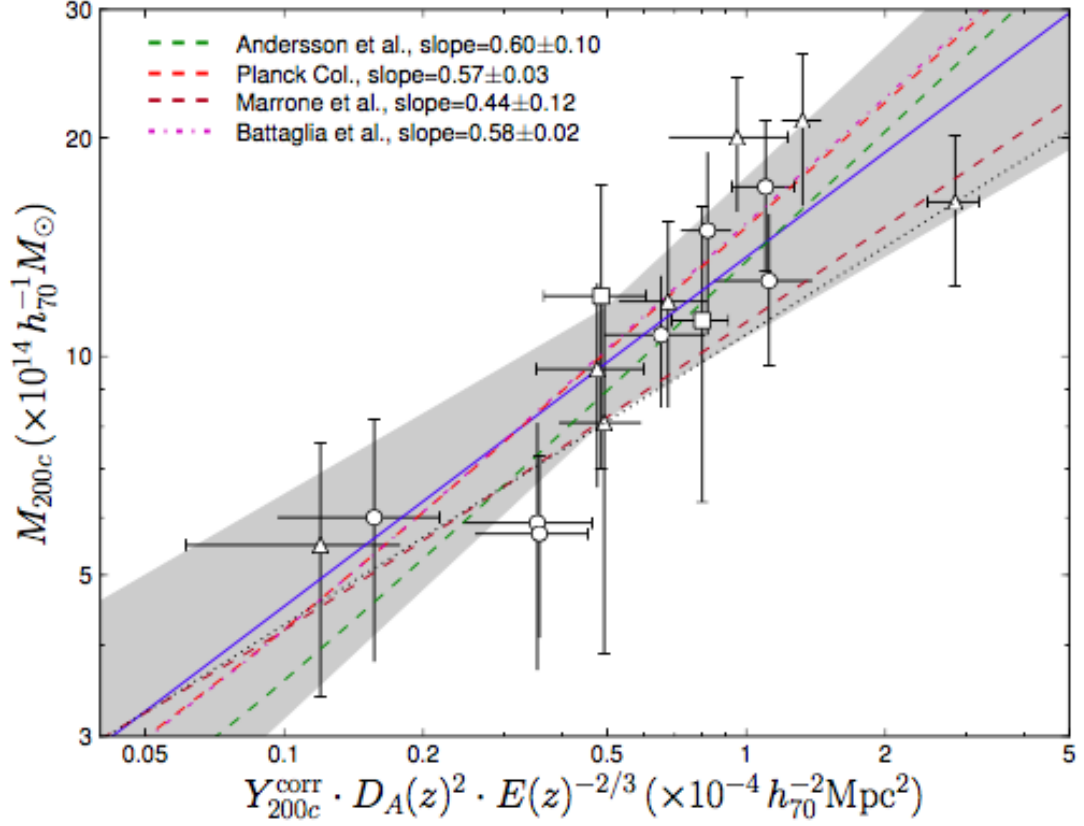


Figure 1.7: Scaling relation plot between dynamical mass (M_{200c}) vs. SZ signal (Y_{200c}) for ACT- detected clusters as measured by [Sifón et al. \(2013\)](#), see text for more details.

Here, $D_A(z)$ is the angular diameter distance in Mpc, $A = 14.99 \pm 0.007$ and $B = 0.48 \pm 0.11$ are the logarithmic normalisation and slope of the scaling relation respectively, and

$$E(z) = [\Omega_M(1+z)^3 + \Omega_\Lambda]^{1/2}. \quad (1.20)$$

Equation 1.19 is a convenient form for parametrising the scaling relation if one wants to predict the mass of a cluster using SZ effect observations.

CHAPTER 2

Cosmological Simulations of Galaxy Clusters

New discoveries and surveys have allowed us to observe the present day and early Universe by observing the CMB radiation along with the current distribution of the Universe with space satellites and ground based telescopes. However, even though observations have shown the shape of the Universe at different times, they are not able to explain the process that transformed the very old small density perturbations into the structures we see today (i.e large scale structures). Cosmologists and astronomers need methods that which can bridge the gap that exists between theory and observations. Most of the information we know today about the Universe arrives to us through light and most of these objects are millions of light years away from our own galaxy. Alternative methods are required in order to solve these problems, some of these problems can be solved by numerical simulations of structure formation of the observable Universe created using powerful super computers.

Cosmological numerical simulations of the Universe have greatly improved our understanding of the physics of galaxy formation. They are widely used to guide the interpretation of the observations, and the design of new astronomical instruments for observations.

Simulations of the Universe play a pivotal role for studies of cosmic structure formation, and they have become a very powerful tool for testing observational techniques used to find galaxy clusters. These methods have provided insight into the distribution of DM, which is not possible to observe, and have been every effective in calibrating new ways of measuring cosmological parameters. Simulations have been crucial in testing the viability of cosmological models of structure formation, such as the cold dark matter (CDM) model and its other forms.

Numerical simulations do come with their own set backs even though they are very good tools for testing cosmological models. One of the challenges is that simulating the visible Universe is much more complex, because it is difficult to model many of the deep astrophysical processes, such as star formation, as a result of poorly understood details of the gas physics. No cosmological simulation is able to resolve the scales needed to properly simulate feedback by active galactic nuclei (AGN) and star formation that are needed to solve the “overcooling problem”, which otherwise leads to simulations producing more stars than are observed. Because of the scope of this project, we are not able to cover the details of all the physical processes modeled in numerical simulations of galaxy clusters. Here we only present a brief introduction to the general aspects.

Theoretical cosmologists have over the past years developed a wide range of different numerical techniques to model galaxy clusters. Cosmological numerical simulations can be divided into two main groups, that is N-body simulations and hydrodynamic simulations. The N-body methods are particle based, but can include a mesh for the solution of the gravitational potential. N-body simulations codes are simulations with discrete number of dynamical system of particles, usually under the influence of gravity. The N-body simulations have been essential for determining the properties of dark matter holes. Previous hydrodynamical simulations of galaxy formation have been based on the smoothed particle hydrodynamics (SPH) technique (Lucy 1977; Gingold & Monaghan 1977; Monaghan 1992, 2005), where gas is discretised into a set of particles.

A lot of observed and some unseen astrophysical phenomena involve complicated interaction processes on a wide range of scales. These astrophysical phenomena are very difficult to probe with astronomical instruments, but with numerical simulations, we can build a picture of the linear-to-non-linear regime of the universe, and build an understanding of the physical processes involved, while making a connection with current observations. Cosmological simulations play a perpetually vital part in theoretical studies of structure formation process in the Universe and without numerical simulations, the Λ CDM model may not have come into being the main theoretical paradigm for structure formation which it is today. The Λ CDM model is the standard modern theoretical foundation for understanding the formation of structure in the Universe (see, Dunkley et al. 2009), it provides the most accepted background for studying the process of cosmic structure formation in the Universe.

In the early 1980s there was lot of growth leading to very important developments for simulations of cosmic structure formation. One of the most widely accepted models for large scale structure formation involves CDM. Right after the innovation of CDM by Blumenthal et al. (1984); Primack & Blumenthal (1984) within a short space of time soon led to one of the very first CDM N-body cosmological simulations (e.g., Davis et al., 1985; Melott et al., 1983). The Λ CDM model assumes that structure grew from weak density fluctuations which happened in the early Universe shortly after the Big Bang, and the Universe has been expanding ever since at an accelerating rate.

Millennium Gas Simulations (MGSs)

For the past several years, one of the most used N-body large simulation of cosmic structure formation for comparing with galaxy cluster surveys has been the Millennium Run Simulation (MS hereafter, Springel et al., 2005) which followed more than 10^{10} particles of mass

$8.6 \times 10^8 h^{-1} M_{\odot}$ of DM distribution within a simulation volume of $(500 h^{-1} \text{Mpc})^3$ from redshift $z = 127$ to $z = 0$. MS was the largest ever simulation of the formation of structure within the Λ CDM cosmology at the time it was published. It was run by an international group of astrophysicists called the Virgo Consortium. The MS was run using the first-year cosmological parameters from the Wilkinson Microwave Anisotropy Probe (WMAP1, see [Spergel et al., 2003](#)) with modified version of a publicly available code GADGET-2 by [Springel \(2005\)](#). These parameters are now known to be incompatible with current measurements of the cosmological parameters.

Galaxy cluster formation is commonly governed by gas that is transformed into forming stars and there needs to be a physical mechanism that allows the stars to become gravitationally bound. The original MS was dark matter only, whereas the Millennium Gas Simulations (hereafter MGSs, [Kay et al., 2012](#)) from the Millennium Gas Project are hydrodynamical simulations which include gas physics.

For this project we used a simulation that had the above mentioned physical applications applicable to it with more gas physics. Our sample of the simulated cluster and galaxy catalogues were drawn from the MGSs, which is a set of large N-body/hydrodynamic (which was the largest of its kind at its time of release) cosmological simulations with flat Λ CDM cosmology with the following cosmological parameters: $\Omega_m = 0.25, \Omega_{\Lambda} = 0.75, \Omega_b = 0.045, h = 0.73, \sigma_8 = 0.9$. The MGSs had an inclusive model added to them for feedback which was implemented using a hybrid procedure with input of energy into the intracluster gas from supernovae (SNe) and AGNs both taken from a semi-analytic model for galaxy formation. This was done to make sure that the MGSs eventually came close to match realistic observations of the observational Universe.

The MGSs (see, [Hartley et al., 2008](#); [Kay et al., 2012](#); [Short et al., 2010](#); [Stanek et al., 2009](#); [Young et al., 2011](#)) are a re-simulations of the original $500 h^{-1} \text{Mpc}$ volume Millennium Simulation (MS, [Springel et al., 2005](#)) with an inclusion of different gas dynamics:

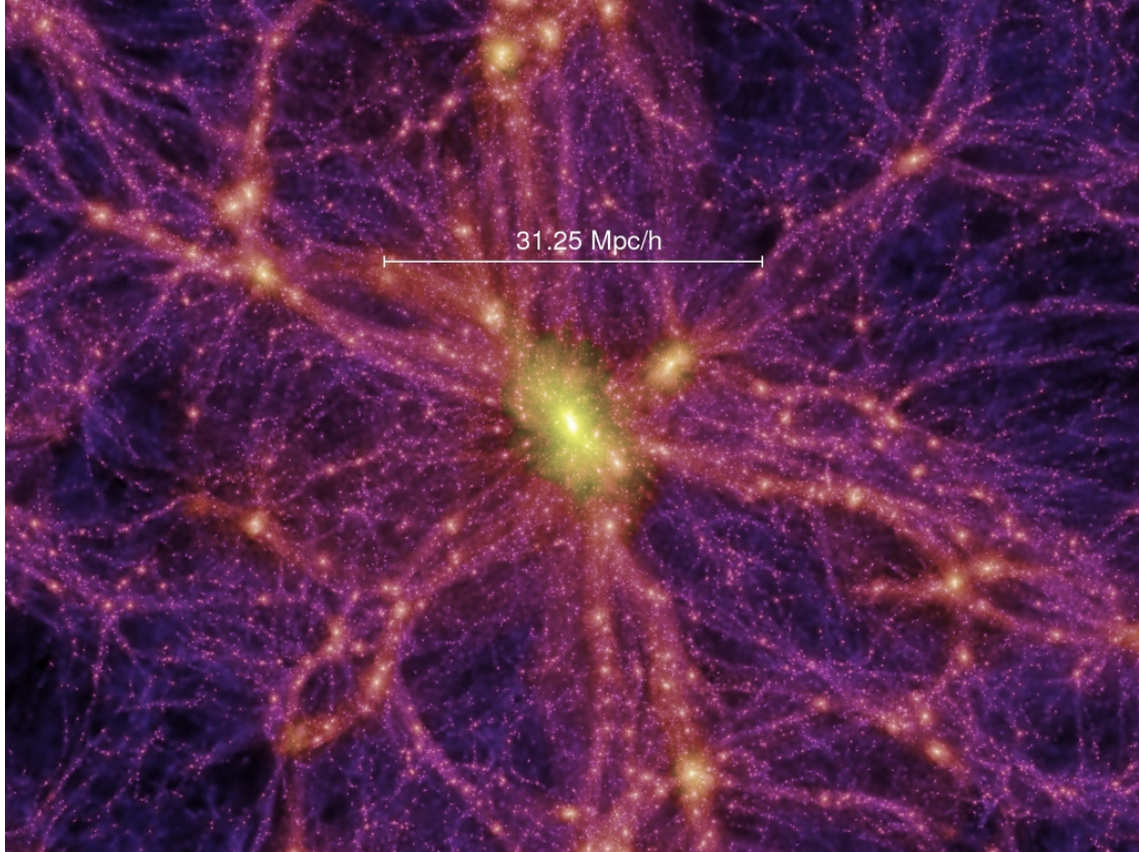


Figure 2.1: The image gives a visual impression of a simulated Universe, a small part cut from the full volume from the Millennium Run Simulation (MS) showing the DM structure distribution on large scales at present epoch ($z=0$). The purple colour represents 'Cosmic Web' which connects individual galaxies, groups and clusters by filaments of the DM (in bright yellow), surrounded by large underdense voids (in black). Image from <http://wwwmpa.mpa-garching.mpg.de/galform/virgo/millennium/>

heating driven by gravity only (GO), cooling and preheating (PH) and a more realistic treatment of feedback (FO), both from SNe and AGNs (Short et al., 2010). These models were added to provide a hydrodynamic version of the Virgo Consortium’s dark matter of the MS. The simulations were run with the publicly available GADGET-2 N-body/hydrodynamics code (Springel et al., 2005). Due to the fact that it was going to be too computationally expensive to do a full run on the whole MS due to the inclusion of gas physics particles, the MGSs was run with fewer particles. The initial conditions were the same as those of MS as described in Hartley et al.(2008), so the particle masses were set to 5×10^8 dark matter particles, each with $m_{dm} = 1.4 \times 10^{10} h^{-1} M_{\odot}$ and 5×10^8 smoothed particle hydrodynamics (SPH) gas particles, each with $m_{gas} = 3.1 \times 10^9 h^{-1} M_{\odot}$. This resulted in mass resolution much more crude than in the original Millennium Simulation.

The Kay et al. (2012) paper on the MGSs builds on the work done by Stanek et al. (2010), where they presented results for SZ $Y - M$ relations for clusters but focused on general issues of multivariate scaling relations. The simulations from Stanek et al. (2010) were performed with gas dynamics under two different physical treatment: GO and PC. In order to have a good theoretical interpretation of SZ cluster samples at high and low redshift with varying gas physics so that the MGSs reassembles the real observable SZ cluster properties closely matched with real observations. A third model (FO) was added to the MGSs used by Kay et al. (2012). The FO includes a more realistic treatment of feedback, both from supernovae and active galactic nuclei (AGNs), it uses the semi-analytic galaxy formation model of De Lucia & Blaizot (2007), run on DM only resimulations of MS clusters, to provide information on the effects of star formation and feedback on the intracluster gas. A snapshot of various properties of the galaxies such as their position, stellar mass and black holes mass are stored in the MGSs.

There are three distinct components of the FO simulation run: hydrodynamical cluster resimulations to track the effect of energy feedback from galaxies on the thermodynamical properties of the ICM, DM only cluster resimulations of each region containing a cluster

from the sample and feedback from semi-analytic galaxy catalogues built on the halo merger trees of these resimulations. The full details of each stage explaining how the FO model was applied to MGSs clusters is discussed in [Short et al. \(2010\)](#). The FO model successfully generates the required excess entropy of the low-redshift population and provides a good match to the structural properties of non-cool-core clusters. [Kay et al. \(2012\)](#) presented results between the SZ Y parameter and cluster observables, and demonstrated that the SZ Y parameter is reasonably insensitive to changes in gas physics that predominantly affect the cluster core. The aim of the MGSs was to focus in more detail on the prediction of the SZ effect, and in particular the $Y - M$ relation for clusters and compare the results to those from other groups using different simulations and observations. The $Y - M$ scaling relations predicted using PC and FO models from [Kay et al. \(2012\)](#), see [Figure 2.3](#), were found to be in excellent agreement with the analysis of [Planck Collaboration et al. \(2011\)](#).

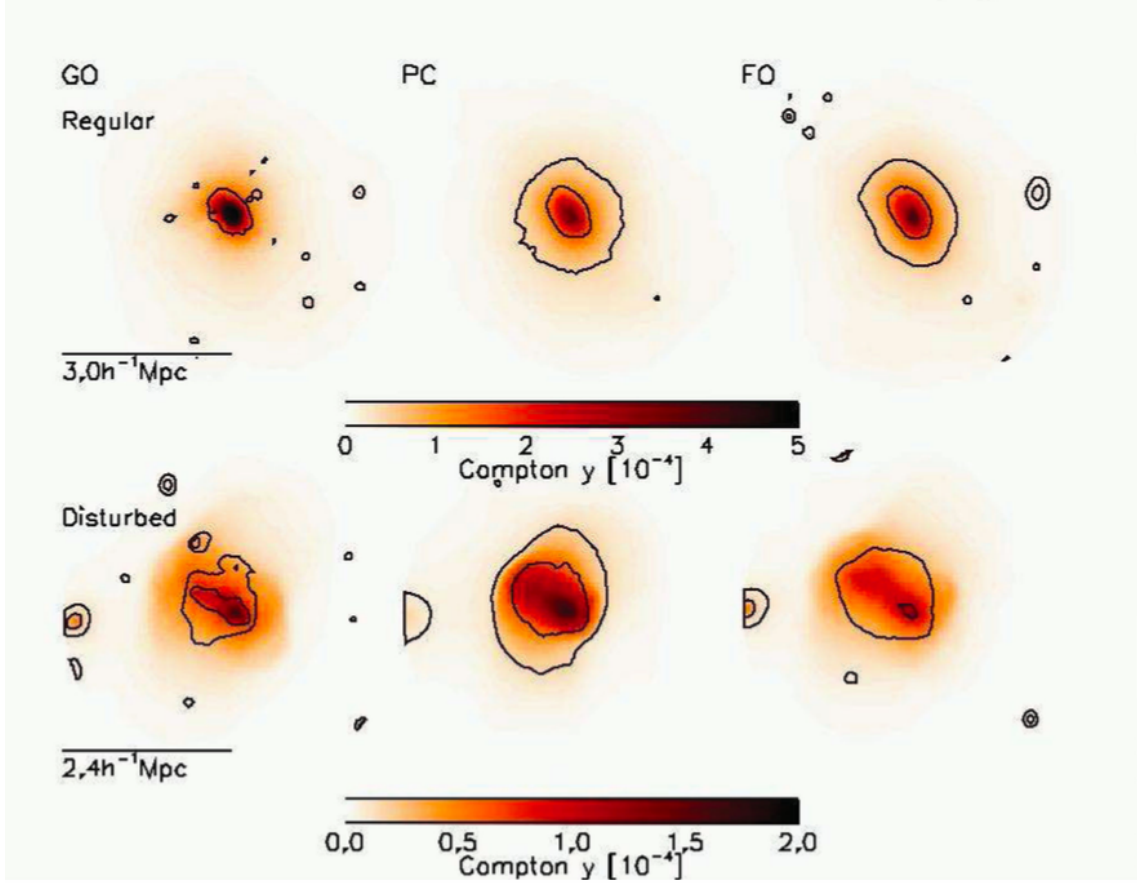


Figure 2.2: Top panels: shows the integrated Compton- y parameter maps determined by the thermal structure of the ICM for most massive clusters ($M_{vir} \simeq 2.9 \times 10^{15} h^{-1} M_{\odot}$) at $z = 0$ in the MS which was classified to be a regular cluster, and from left-hand side to the right-hand side we can see the results which was found for the GO, PC and FO simulation respectively. The images in the bottom panel show similar results but for disturbed clusters (with $M_{vir} \simeq 1.5 \times 10^{15} h^{-1} M_{\odot}$). The above results were found by [Kay et al. \(2012\)](#) using the MGSs.

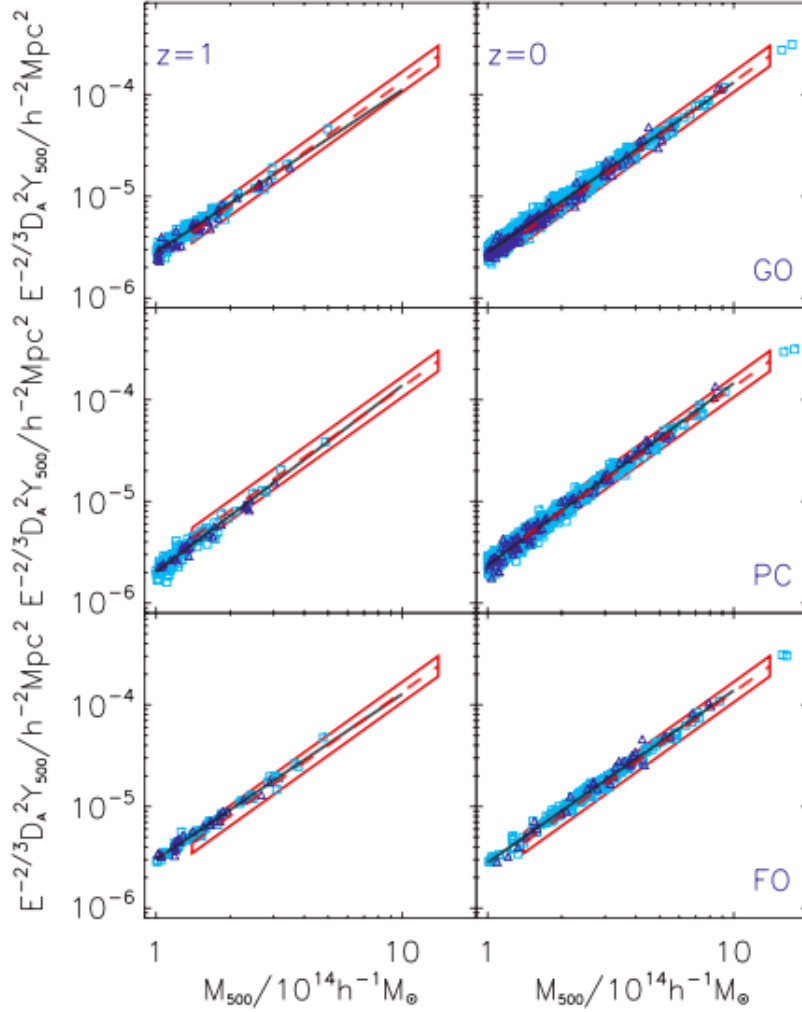


Figure 2.3: Scaling relations between the SZ flux, Y_{500} , and total mass, M_{500} , for the GO (top panels), PC (middle panels) and FO (bottom panels) models at $z = 1$ (left-hand panels) and $z = 0$ (right-hand panels). The solid diagonal line is a least-squares fit to the relation. The best-fitting power law to $z < 0.5$ Planck/XMM-Newton combined data from [Planck Collaboration et al. \(2011\)](#) is shown in all panels as a dashed line, while the box illustrates the intrinsic scatter in the observed relation. The triangles represent disturbed clusters, while the squares are regular clusters. The above image and results were found by [Kay et al. \(2012\)](#) using the MGSs.

CHAPTER 3

Mock SALT cluster observations and analysis

In this chapter we describe cluster and galaxy simulations used to make mock galaxy cluster catalogues that we used to mimic real observational methods. We also present methods used for determining cluster membership in order to make measurements of the velocity dispersion and scaling relations used to estimate the dynamical mass of each cluster.

To make the mock galaxy cluster catalogues, we follow the same procedure as in [Kirk et al. \(2015\)](#) which describes SALT follow-up observations of galaxy clusters detected by ACT ([Hasselfield et al., 2013a](#); [Menanteau et al., 2013](#)). This is important for future studies of ACT clusters that aim to use SALT for much larger studies of dynamical mass measurements. From [Kirk et al. \(2015\)](#), we know that SALT can target ~ 25 galaxies per slit mask, and our ultimate aim for this project is to answer the question: for a fixed amount of telescope time, is it better to obtain many low quality velocity dispersion measurements, or fewer, higher quality velocity dispersion measurements? That is, how many masks per cluster should be used to make a reasonable measurement of the $Y - \sigma_v$ relation (see Chapter 4)?

In this chapter we will describe how to make mock observations and analyse them (measuring the velocity dispersion). We use the completeness limits estimated from SALT (from, [Kirk et al., 2015](#), see Figure 3.2 below here) to determine the redshift success rate of our mock galaxy clusters catalogues from MGSs. We begin with a brief introduction to SALT multi-object spectroscopy (MOS).

3.1 South African Large Telescope (SALT) Multi-Object Spectroscopy

The Southern African Large Telescope (SALT) is a 11-metre optical telescope located in Sutherland, South Africa, and is operated by the South African Astronomical Observatory (SAAO). The Robert Stobie Spectrograph (RSS) of SALT was designed with spectropolarimetric versions of all its modes which provides capabilities of making multiple object measurements referred to as Multi Object Spectroscopy (MOS) (Nordsieck et al., 2001), and is able to make measurements from 3200–9000 Å (where 1Å = 10⁻⁸ cm). MOS offers the possibility of obtaining spectra of about 25 objects simultaneously, if 10'' long slits are used.

RSS can be operated in MOS mode using custom made slit masks which are laser cut. The RSS has a circular 8' field of view, which is well matched to the sizes of clusters at intermediate redshift ($z > 0.3$).

For MOS observations, the observer will do pre-imaging before conducting an actual observation and pre-imaging is normally done in the field-of-view of the telescope. In [Kirk et al. \(2015\)](#), Sloan Digital Sky Survey (SDSS) imaging was used in the preparation of the slit masks and once mask design is done they cannot be changed during actual observations. SDSS is a major multi-filter imaging and spectroscopic redshift survey using a dedicated 2.5m wide range-angle optical telescope (see, [Gunn et al., 2006](#), for more details) at Apache

Point Observatory (APO) in the Sacramento Mountains in Southern New Mexico. SDSS has been in operation since year 2000 April and has created one the most detailed 3D maps of the Universe ever made (see, [Aihara et al., 2011](#)). It has made photometric observations of around 500 million objects and spectra of more than 3 million objects.

[Kirk et al. \(2015\)](#) reported observations of seven clusters that had previously been detected by ACT ([Hasselfield et al., 2013a](#); [Menanteau et al., 2013](#)). The clusters were detected in SZ with $4.6 < S/N < 8.3$, and were selected to be $z \approx 0.4$, to make sure that the targeted galaxies would have bright enough absorption lines for successful redshift measurements, given the capabilities of the RSS instrument of SALT at the time of observation.

Figure 3.1, shows an example of a slit mask finder chart for mask 1 covering ACT-CL J2058 as in [Kirk et al. \(2015\)](#). The green rectangles are slits placed on galaxies and the red square boxes for alignment stars. During acquisition at SALT, slits were placed on 3–4 bright stars per cluster field to help optimise the final alignment. The slit masks were designs with images acquired from (SDSS [Aihara et al., 2011](#)) the 8th data release (DR8, hereafter). The mask design have geometric constraints in order to avoid overlapping spectra and to ensure the necessary wavelength coverage is met. The slitlets had dimensions of; length = $10''$, width = $1.5''$ and the minimum safety fixed gap that was left between the slits was $1.0''$, to avoid any superposition of spectra. These dimensions were chosen because SALT is located at Sutherland where the median seeing is $1.3''$ (see, [Catala et al., 2013](#)). The slitlets used were able to target between 19–26 galaxies in each cluster field per slit mask ([Kirk et al., 2015](#)).

The slit mask was centred on the Brightest Cluster Galaxy (BCG), using the coordinates listed in [Menanteau et al. \(2013\)](#). Target galaxies were selected to be fainter than the BCG and with colour bluer than the estimated redward edge of the red-sequence. The red-sequence defines a tight relationship between magnitude and colour, and is mostly followed by elliptical galaxies (see, e.g, [Rykoff et al., 2014](#)). The slits were assigned to galaxies

in an automated way that prioritised objects closer to the cluster centre. This was done to ensure the number of objects whose spectra were centred horizontally on the detector array was maximised.

Figure 3.2 shows the fraction of successful redshift measurement as a function of galaxy r-band magnitude range 17.9–23.9, for all the galaxies which were targeted by Kirk et al. (2015). The design of SALT limits observations on the celestial equator to tracks of 3200 sec duration. The graphs in the upper panel show the magnitude distribution of the target galaxies. The galaxy redshift was measured by cross-correlating the spectra with SDSS galaxy spectral templates using the RV SAO/XCSAO package for IRAF (Kurtz & Mink, 1998), the cross-correlation was run repeatedly in intervals of $\partial z = 0.0001$ spanning between redshifts of $0.0 < z < 1$ for 6 different templates. Out of the 372 galaxies which were targeted, 191 of them were successfully measured (51% z success rate) as some of the galaxies were very faint.

In Section 3.3.1, we describe how we constructed mock slit mask observations from the Millennium Gas Simulations.

3.2 Cluster Sample

To simplify the analysis, we used a galaxy and cluster catalogue from the MGSs, extracted at $z = 0$. This allowed us to neglect any evolution in cluster properties. Our galaxy cluster catalogue was taken from the FO run model of the MGSs which are appropriate to use when analysing the SZ properties for individual clusters.

We define M_{500} (M_{200}) in M_{\odot} as the mass of the clusters contained within the characteristic radius R_{500} (R_{200}) in Mpc, the radius from the cluster center within which the

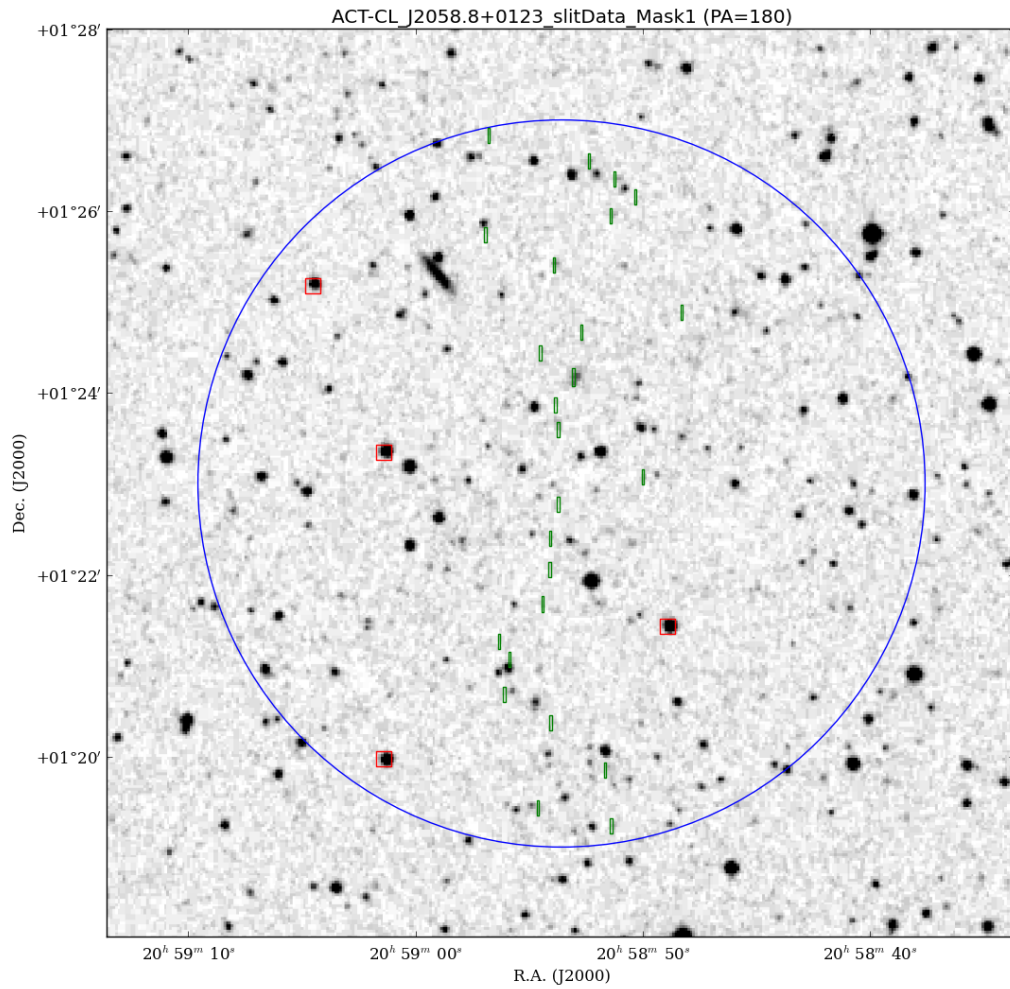


Figure 3.1: Finder chart for an example SALT slit mask design, the red square boxes are placed on the brightest stars for alignment and the green rectangles are the slits placed on galaxies. This chart was done for ACT-CL J2058 cluster using 1 mask as in [Kirk et al. \(2015\)](#).

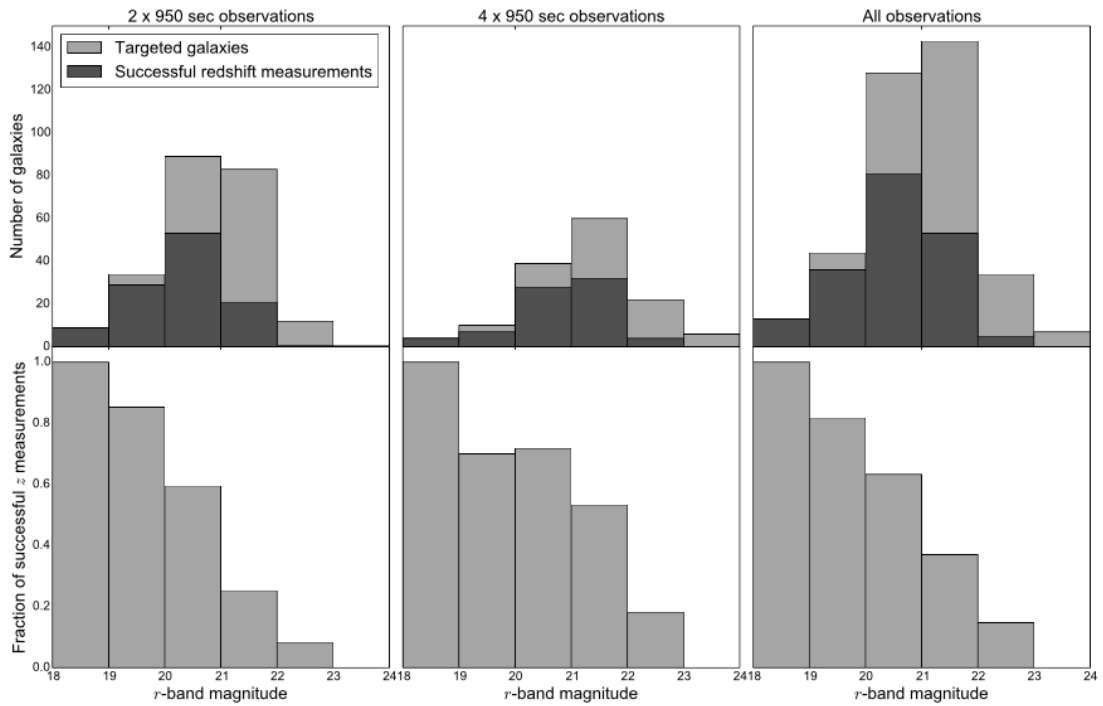


Figure 3.2: SALT redshift (z) success rate for galaxies targeted by Kirk et al. (2015) during observation. The results of the graph above show the z success rate as a function of r -band magnitude for 2×975 sec of integration in column 1, 4×975 sec in the second column, and for all observations shown in the last columns.

average density is 500 (200) times the critical density at the cluster redshift z , where

$$R_{500} \approx 0.6 \times R_{200}, \quad (3.1)$$

and R_{200} is roughly the virial radius.

Cluster properties stored in Millennium Gas Simulations catalogue

In the MGSs (from, [Kay et al., 2012](#); [Short et al., 2010](#)) various properties are stored in snapshots, these include, from the cluster catalogue; the identification number (ID) for each cluster, mass of the cluster M_{500} (in $h^{-1} M_{\odot}$) within the characteristic radius R_{500} (in h^{-1} Mpc), the position coordinates (units in h^{-1} Mpc) of the cluster centre giving the location of the cluster in the simulated Universe. The simulated cluster catalogue also has measurements of the three dimensional (3D) velocity dispersion (σ_{3D}) of the total cluster mass distribution. Since we want to compare this with our own recovered one dimension (1D) LOS velocity dispersion σ_v , we assume an isotropic velocity distribution in converting σ_{3D} using the equation below,

$$\sigma_{1D} \equiv \frac{\sigma_{3D}}{\sqrt{3}}. \quad (3.2)$$

Another very important cluster property, included, is the frequency-independent SZ Comptonization (Y_{500}) parameter given by

$$Y_{500} = \frac{1}{D_A^2} \frac{\sigma_T}{m_e^2} \int n_e k_B T_e dV, \quad (3.3)$$

integrated within R_{500} and Y_{500} is normally measured in steradians, which we convert into an intrinsic Y_{500} (which takes out the surface brightness dimming effects) by multiplying by D_A^2 (cosmology dependent), i.e., the angular diameter distance to the cluster. Hence $Y_{500} D_A^2$ has units of h^{-2} Mpc². In the MGSs the value of Y_{500} is estimated for each cluster using

$$Y_{500} = \left(\frac{\sigma_T k_B m_{gas}}{\mu_e m_H m_e c^2} \right) \sum_{i=1}^{N_{hot}} T_i, \quad (3.4)$$

where the mean molecular weight per electron is $\mu_e = 1.14$, which is suitable for a fully ionised plasma of hydrogen, assuming $T = T_e$ (equipartition of energy between the electrons and nuclei) and the summation runs over all hot ($T > 10^5$ K) gas particles within R_{500} , with mass m_{gas} and temperature T_i .

The simulated galaxy catalogues consists of; the ID's for each galaxy, the position coordinates (in units Mpc) of galaxies inside the simulated Mpc box, which are used to match against the simulated clusters center position coordinates, the components of the galaxy velocity (in units km s^{-1}) in each axis, and the absolute magnitudes of the galaxy in SDSS photometric bands (u, g, r, i, z: see <http://www.sdss.org/>). These are used to pick, e.g., the magnitude limited galaxy samples.

3.3 Data Analysis and Results

In this section we going to describe the methodology used to make measurements of cluster properties: velocity dispersion, and dynamical mass. Making these measurements it is very important to accurately determine cluster membership to avoid biased measurements of the velocity dispersion and cluster mass. We calculate the velocity dispersion of each cluster using a software developed by [Wilson et al. \(2015\)](#) and use scaling relations we derive from MGSs and [Munari et al. \(2013\)](#) cluster mass relation to estimate the cluster dynamical mass. The data analysis methods we use are very similar to the ones used in [Kirk et al. \(2015\)](#). We use these observational methods to make mock cluster catalogues to mimic a realistic observation similar to the one SALT conducted when follow-up observations were done on clusters which had been detected by ACT on the celestial equator using the SZ effect. SALT conducted a MOS (which uses custom designed slit mask) observations with the RSS in order to measure galaxy redshifts in each cluster field to determine the cluster velocity dispersion in LOS. The LOS velocity dispersion is used to infer cluster dynamical mass by using scaling relations obtained from zoomed-in N-body/hydrodynamical simulations of dark matter halos, that includes prescriptions for cooling, star formation, and

AGN feedback (e.g [Munari et al., 2013](#), and from MGSs).

3.3.1 Extraction of Simulated Galaxy and Cluster Catalogues from MGSs to mimic real Cluster Catalogues

All of our data analysis was done using Python 2.7 (see, <https://www.python.org/>), a high level programming language. The Python 2.7 program is widely used for astronomical data analysis and is a free open-source software which also has a community-based development model. All the extra packages needed for data processing were preloaded into our python library database. We wrote a Python code that allowed us to extract the simulated cluster and galaxy catalogues of the MGSs which are in Flexible Image Transport System (FITS) format.

We use the MGSs simulated cluster and galaxy catalogues for $z = 0$, a different number of clusters were randomly selected, and only clusters with $\log_{10}(M_{500}/M_{\odot}) > 13.8$ were considered. For the purposes of our study, we assume that evolution is negligible and artificially redshift the cluster galaxies to $z = 0.3$, this is better matched to the observations described in [Kirk et al. \(2015\)](#) and is well matched to SALT's 8' field of view. We also convert the provided galaxy absolute magnitudes (u, g, r, i, z: M) to apparent magnitudes (m) for all the galaxies using

$$m = 5(\log_{10}(Dl \cdot 10^5)) + M, \quad (3.5)$$

where the luminosity distance $Dl = 1552.673$ Mpc. We convert the physical distances recorded in the X, Y axes of the MGSs into angular distances by adopting a scale factor of 0.062 deg/Mpc. In Equation 3.5 we neglected the k-correction because it is small for our simulated observations (0.12 mag for an early-type galaxy at $z=0.3$).

Our new data was arranged accordingly and saved into new text-files that we later fed

into a software that is used to read the galaxy catalogs and make files for importing into the SALT RSS slit making tool, similar to the ones used for real targets when conducting observations with SALT (e.g [Kirk et al., 2015](#)).

Figure 3.3 shows a colour-magnitude diagram for one of the MGS clusters. The red dots represent galaxies selected for inclusion in a mock observation slit mask, while the blue dots represent all other galaxies within the vicinity of the simulated cluster. To make sure all the galaxies targeted are fainter than the BCG and with colour bluer than our estimate of the red-edge of the red-sequence, we set target cuts for top priority targets to put slits on galaxy apparent magnitudes; $i > 17.9'$, $g-r < 2.0'$, $i < 22'$ and the galaxies that passed the target cuts are placed in a mask. We also apply secondary targets, these are used when no more of the galaxies that pass target cuts can be placed in a mask; $i > 17.9'$, $i < 23'$. Multiple masks (1-4) were generated for each cluster in the sample. The masks are labelled in a simple way: masks used in run 1 are called mask 1, while a different number masks used in run 2, 3 and 4 are called mask 2, 3 and 4 respectively.

3.3.2 Determining Galaxy Cluster Members

It is very important to deduce as accurately as possible the true galaxy cluster membership to avoid biased measurements of the velocity dispersion. Deducing which galaxies are true members of the cluster is often tricky due to interloping galaxies that appear along the LOS. To find and remove interlopers we apply a rejection method referred to as the shifting gapper method developed by [Fadda et al. \(1996\)](#) and was further refined by [Crawford et al. \(2014\)](#) to identify cluster members. Our approach is similar to the procedure implemented by [Wilson et al. \(2015\)](#).

We first calculated the peculiar velocity for galaxies relative to our estimate of cluster redshift, where for all the clusters an estimate of the redshift is known since we artificially redshift the cluster of galaxies to $z = 0.3$ and this is used as a starting point. The peculiar

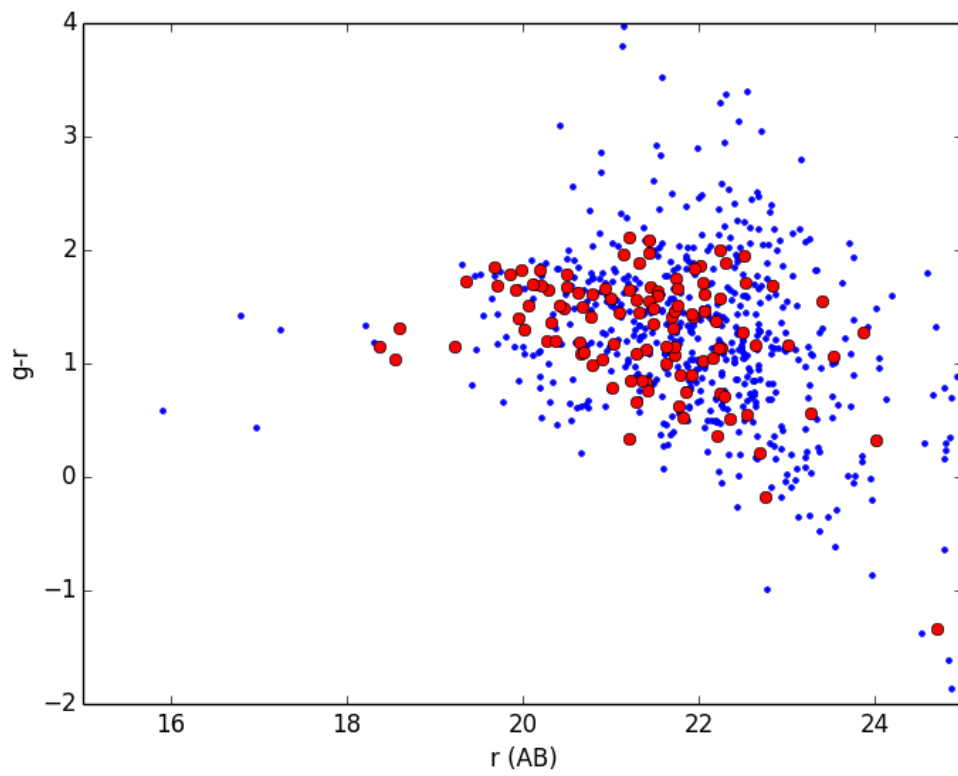


Figure 3.3: Image of all the galaxies that were selected in blue circle dots, and the red ones are those selected in the 4 slit masks (see text for more details)

velocity Δv_i of each of the galaxies is calculated relative to this redshift estimate and we define it as

$$\Delta v_i = c \frac{z_i - \bar{z}}{1 + \bar{z}}, \quad (3.6)$$

where the Δv_i is the peculiar velocity of the i^{th} galaxy, z_i is its redshift, and \bar{z} is the cluster redshift (0.3) and c is the speed of light. We calculate the peculiar velocity of each individual galaxy, and in order to reject possible non-cluster members for our samples from the mock catalogues, we adopt the following procedure; we remove all the galaxies with $\Delta v_i > 3000 \text{ km s}^{-1}$ or $< -3000 \text{ km s}^{-1}$ with respect to the cluster redshift, and this process was iterated until convergence was reached.

[De Propris et al. \(2002\)](#) found that galaxy clusters correspond to well-defined peaks in the distribution of galaxy recessional velocities, and that gaps of more than 1000 km/s between adjacent galaxies indicates the presence of interlopers. To exclude them, we sorted all galaxies by their peculiar velocities and identified any galaxies with gaps differing by more than 1000 km s⁻¹ adjacent to each other. We iteratively removed all galaxies with gaps greater than 1000 km s⁻¹ compared to their nearest adjacent neighbour in velocity space until the number of galaxies in the cluster reached convergence. The fixed optimum gap (1000 km s⁻¹) found by [De Propris et al. \(2002\)](#) is adequate because its also avoids the merging of subclusters and prevents the breaking of real systems into smaller groups.

Only galaxies enclosed within R_{200} (the radius within which the mean density is 200 times the critical density of the Universe) were selected and we excluded all galaxies located at a projected radial distance from the cluster centre greater than R_{200} , as these were not considered to be associated with the cluster. To ensure that we did not exclude possible members, we express R_{200} following [Finn et al. \(2005\)](#) as

$$R_{200} = 1.73 \frac{\sigma_v}{1000 \text{ km s}^{-1}} \frac{1}{\sqrt{\Omega_\Lambda + \Omega_0(1+z)^3}} h^{-1} \text{ Mpc}, \quad (3.7)$$

where σ_v is the line of sight velocity dispersion (see, Section [3.3.3](#)) and z is the cluster redshift. In Equation [3.7](#) we assume that the galaxy velocity distribution follows an isothermal

sphere dark matter profile.

Note that in some cases, the procedure of selecting members galaxies returns fewer than 10 members. We exclude these clusters from our analysis (as typically done in observations studies, e.g. [Wilson et al. \(2015\)](#)), as the velocity dispersion measurements may not be robust. As a result, this means that the number of simulated clusters in the sample with either 100% redshift completeness, or realistic redshift completeness, is not always equal.

3.3.3 Recovered Velocity Dispersion

The cluster LOS 1D velocity dispersion (σ_v : in km s^{-1}) was calculated using only galaxies identified as members from the measurements of Δv_i in Section 3.3.2. The velocity dispersion σ_v was computed via the biweight scale estimator (see, [Beers et al., 1990](#)) method; it is an effective statistical estimator for finding the dispersion of Δv_i because it is robust to outliers. The errors were computed via a bootstrap resampling 1000 technique. The bootstrap method does not rely on any prior assumption of the underlying data distribution; therefore it is more robust than traditional error estimators, since the velocity distribution is unknown.

Figure 3.4 shows results for the recovered 1D velocity dispersion (σ_v), calculated from all the galaxies that were selected to be members of the cluster. The graphs on the upper panel show only those which have 100% redshift completeness, since we are dealing with simulations to get such measurements. For real optical observations such as those of [Kirk et al. \(2015\)](#), it is not possible to get 100% redshift completeness of all the targeted galaxy clusters especially for very faint distant galaxy clusters. We show results of σ_v , for a realistic case of redshift completeness in the bottom panel of Figure 3.4, where we applied the same fraction of redshift success rate as it was found by [Kirk et al. \(2015\)](#) (e.g. see, Figure 3.2 column one bottom panel which obtains a 2×975 of integration per mask spanning the r-band magnitude range 17.9–23.9).

Figure 3.4 shows how well σ_v is recovered depending on whether 1–4 masks were used per target and also on the cluster redshift success rate. We define the bias and scatter in the recovered σ_v respectively as the mean and standard deviation of $(\sigma_v - \sigma_{1D})/\sigma_{1D}$ (referred to as ‘mu’ and ‘sigma’ in Figure 3.4). For 100% z success rate, the scatter seems to not change but the percentage of the bias changes from about 2.5%–0.07% when between 1–4 mask used on the clusters. For the realistic case, we see that the scatter ranges from 14–18%, and the percentage of the bias decreases from 5.6% to about 2% when 3 or 4 masks are used. The recovered velocity dispersion is almost unbiased.

3.3.4 Dynamical Cluster Mass Estimates

Using velocity dispersion as a mass proxy, we estimate the total dynamical cluster mass using scaling relations derived from numerical simulations. We also check how the recovered mass changes according to the assumed redshift success rate, and with 1–4 slit masks per cluster target (Figures 3.6 and 3.7).

Figure 3.5 shows a linear regression log-log plot between $M_{500true}$ and σ_{1D} , where $M_{500true}$ is the cluster dynamical mass (in $h^{-1} M_{\odot}$) measured from the MGSs within characteristic radius R_{500} . We compare $M_{500true}$ with our estimated total cluster mass measurements M_{500} and M_{500c} both in units $h^{-1} M_{\odot}$, that is cluster mass estimated from σ_v measurements of galaxies in clusters using scaling relations, to be discussed in more detail later. σ_{1D} (in $km\ s^{-1}$) is the the 1D velocity dispersion of the total cluster mass distribution of galaxies in clusters in the MGSs, calculated using Equation 3.2. The black solid line shows the log-log linear regression best fit line, we use the relation below (Equation 3.8) to get an estimate of the dynamical cluster mass M_{500} given by

$$M_{500} (h^{-1} M_{\odot}) = (\sigma_v (km\ s^{-1}))^{2.94} \times 10^{5.84}, \quad (3.8)$$

for each cluster, and the results of the recovered cluster mass M_{500} are shown in Figure 3.6.

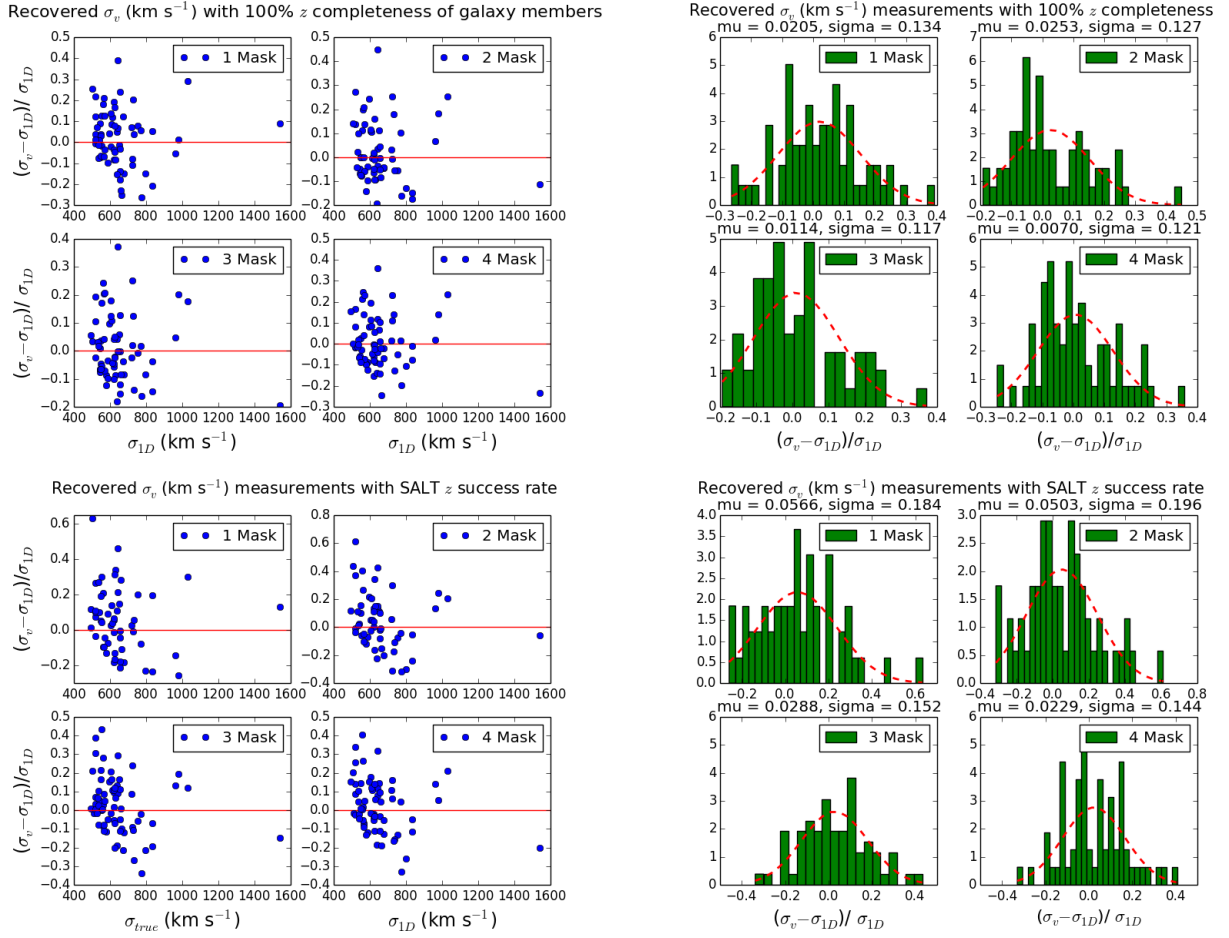


Figure 3.4: The plots above illustrate how well 1D velocity dispersion (σ_v) is recovered from galaxies selected to be true members of a cluster, where 1-4 masks were used per cluster. The top panel shows for 100% z completeness and the bottom for the realistic z completeness. σ_v is the recovered 1D velocity dispersion, σ_{1D} is the known velocity dispersion of the total cluster mass distribution from MGSs, 'mu' and 'sigma' define the bias and scatter of the recovered σ_v respectively. See text for more details.

The mass measurements shown in Figure 3.7 are derived using the relation of [Munari et al. \(2013\)](#), which was calibrated using subhalos and galaxies,

$$M_{200c} = 10^{15} h^{-1} M_{\odot} \times \left(\frac{\sigma_v (km s^{-1})}{A_{1D}} \right)^{1/\alpha} \quad (3.9)$$

where $A_{1D} = (1177 \pm 4.2) \text{ kms}^{-1}$ the normalisation parameter, $\alpha = 0.364 \pm 0.0021$ is the

slope, and the simulation included AGN feedback using galaxies with stellar masses ($> 3 \times 10^9 h^{-1} M_{\odot}$). Since we compare our cluster mass with other relations we convert our M_{200c} estimate into M_{500c} by using the mass-concentration (c-M) relation given in [Duffy et al. \(2008\)](#) assuming a Navarro-Frenk-White (NFW; [Navarro et al., 1997](#)) density profile. The results of the recovered cluster mass (M_{500c}) are shown in [Figure 3.7](#), the top panel shows 100% z completeness, and the bottom panel shows the realistic case for z success rate from SALT.

In [Figure 3.6](#) and [3.7](#) we are measuring the fractional difference by comparing the recovered total dynamical cluster mass (M_{500} , M_{500c}) from galaxies which were selected to be members of a specific cluster with the true total cluster ($M_{500true}$) measured directly from the MGSs. This was done to see how 100% redshift completeness, and realistic redshift incompleteness affects cluster mass measurements when a different number of masks are used. In both figures we can see that the bias for 100% redshift completeness is less than the bias of the realistic redshift incompleteness, which indicates that having good redshift completeness has the potential to improve cluster mass measurements. The right hand side of [Figure 3.6](#) and [3.7](#) on the lower panel for realistic redshift incompleteness show that we over estimate the cluster mass by $\sim 30\%$, $\sim 22\%$, and if we use more masks the bias decreases to $\sim 15\%$, $\sim 11\%$ for [Figure 3.6](#) and [3.7](#) respectively, and the scatter changes by roughly 10% for both figures.

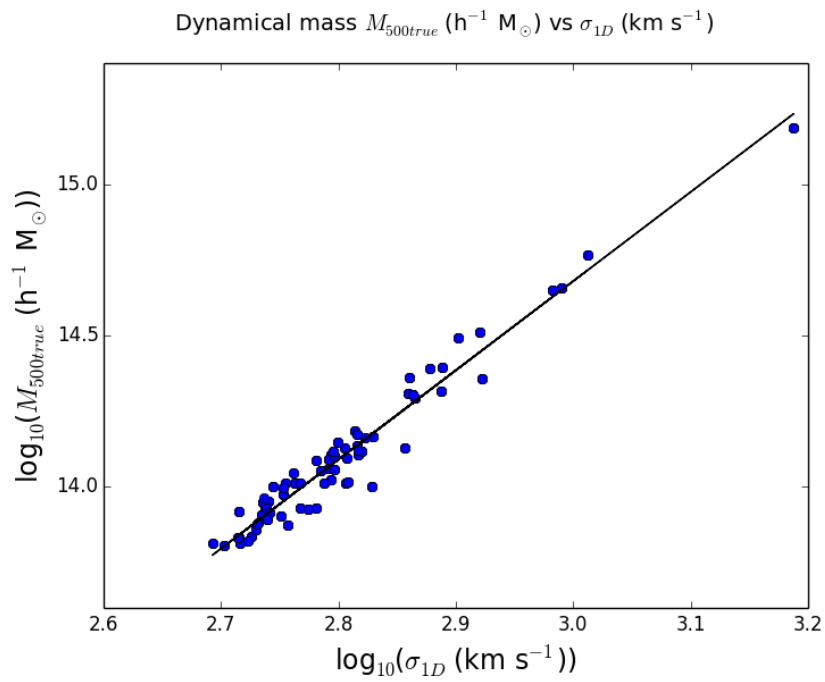


Figure 3.5: Log-log plot of the true values as measured from MGSs of the cluster dynamical mass $M_{500true}$ ($h^{-1} M_{\odot}$) versus 1D velocity dispersion σ_{1D} (km s^{-1}) of galaxy clusters. The black solid line shows the log-log linear regression best line fit. See text for more details

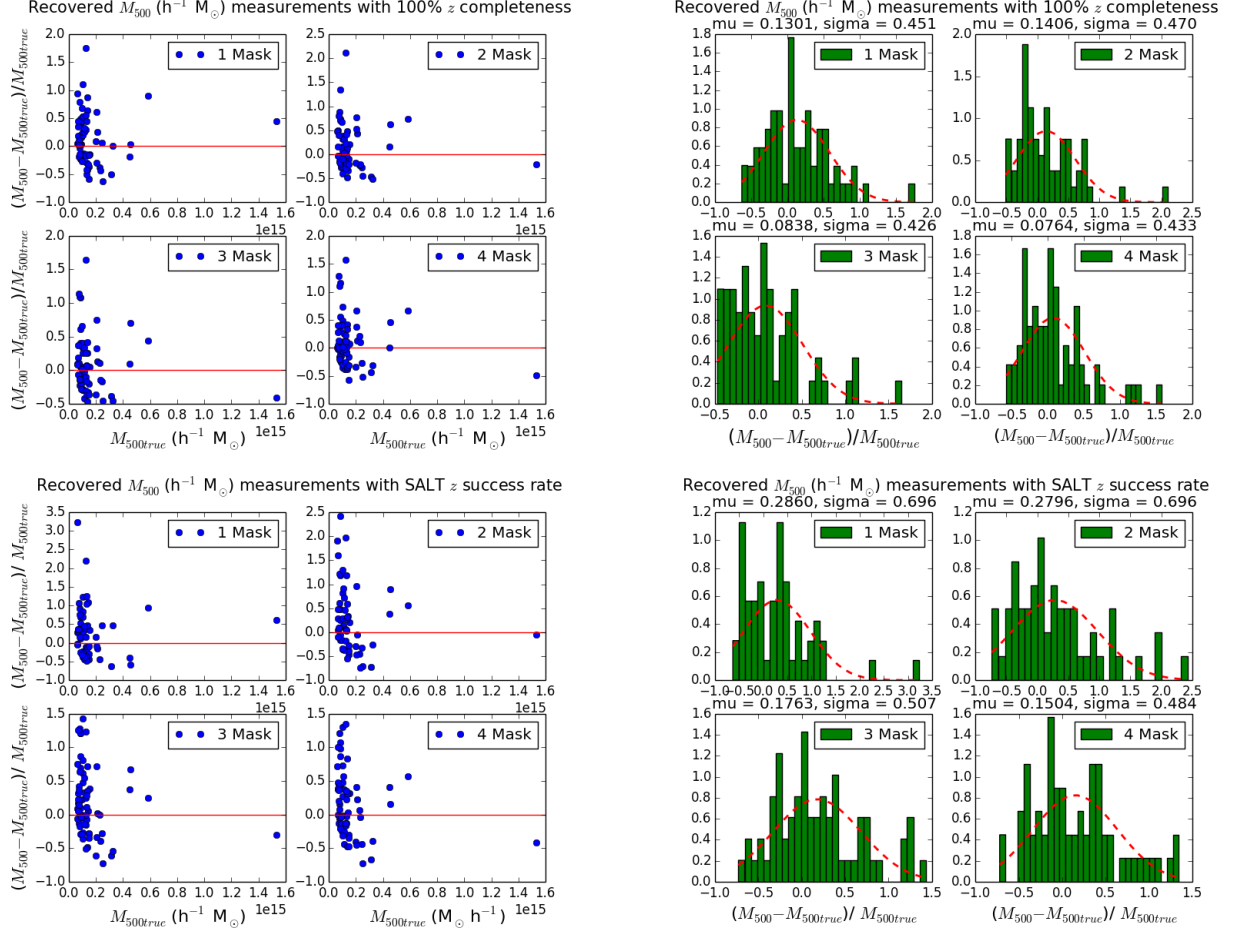


Figure 3.6: The plots above show how well M_{500} is recovered, that is mass estimated from using Equation 3.8 relation by applying the velocity dispersion (σ_v) of galaxies that were selected to be true cluster members, where 1-4 masks were used per cluster. The top panel for shows measurements of 100% z completeness and the bottom for the realistic z completeness. The bias of the estimated cluster mass (M_{500}) is indicated by ‘mu’ and ‘sigma’ gives the scatter. See text for more details.

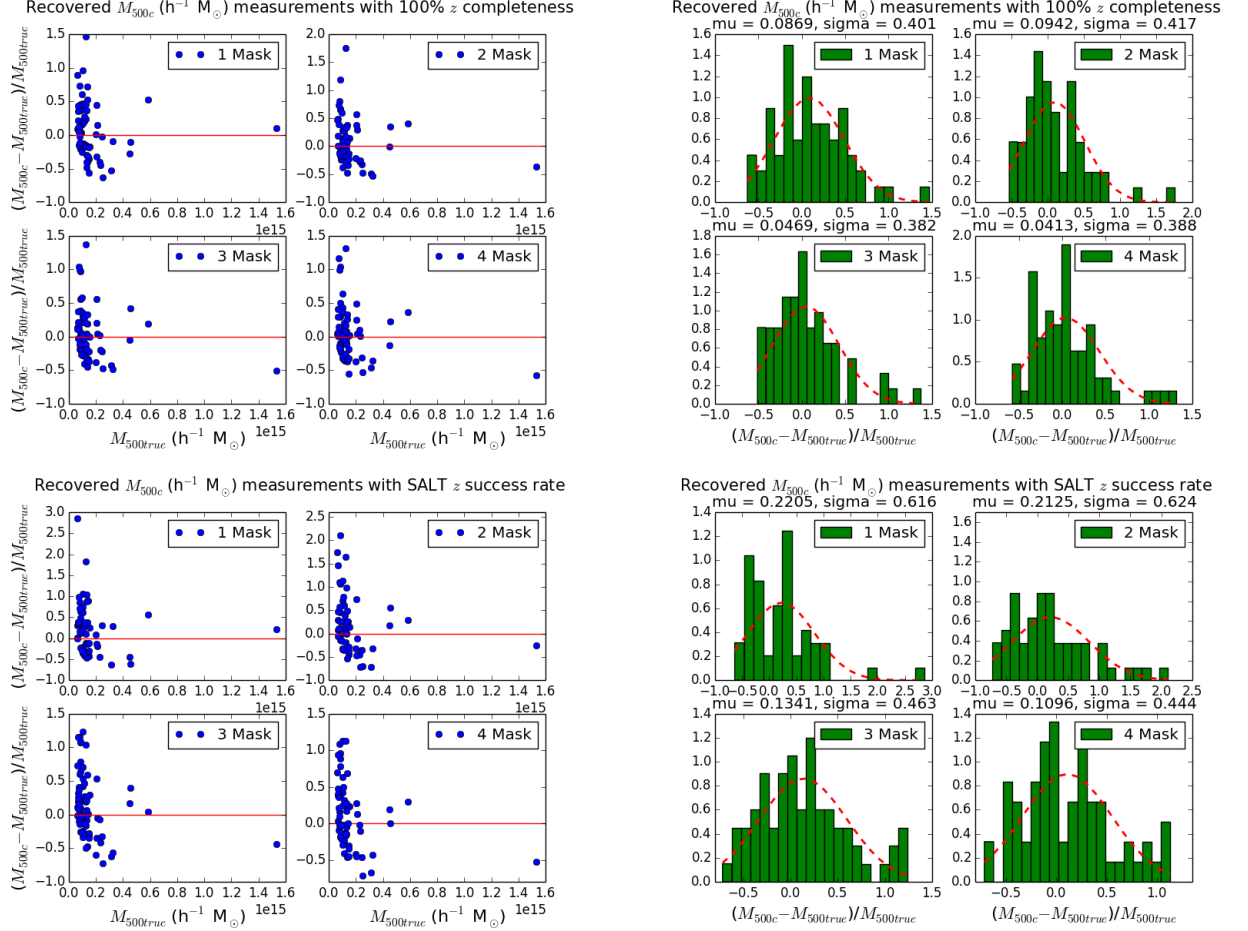


Figure 3.7: The plots above show how well M_{500c} is recovered, that is mass estimated from using the [Munari et al. \(2013\)](#) relation (see, Equation 3.9) by applying the velocity dispersion (σ_v) of galaxies that were selected to be true cluster members, where 1-4 masks were used per cluster. The top panel for shows measurements of 100% z completeness and the bottom for the realistic z completeness. The bias of the estimated cluster mass (M_{500c}) is indicated by ‘mu’ and ‘sigma’ gives the scatter. See text for more details.

CHAPTER 4

SZ Scaling Relations

In this section we focus on the relationship between the SZ Comptonisation (Y_{500}), integrated within R_{500} , and the velocity dispersion of member galaxies. Since velocity dispersion is the measure of the kinetic energy of the galaxies in the cluster and Y_{500} is related to the ICM gas in the cluster, both are good tracers of clusters.

Figure 4.1 shows the scaling relation between SZ signal (Y_{500}) versus 1D velocity dispersion (σ_{1D}) as measured from the Millennium Gas Project simulations we used here (see, [Kay et al., 2012](#)). The solid black line shows a least-square best-fit line to the data, we found

$$Y_{500} D_A^2 = \sigma_{1D}^{5.29} \times 10^{-20.14} \quad (4.1)$$

in log-space where 5.29, -20.14 describe the best-fitting slope (B_{true}) and normalisation respectively. We adopt $B_{true} = 5.29$ as the true measure of the slope for the relation and use it to compare with the recovered slopes (B_{rec}) for $Y_{500} D_A^2 - \sigma_v$ relation, where a different number of clusters were randomly selected and with a different number of masks 1-4 placed to each cluster sample. We obtain $Y_{500} D_A^2 - \sigma_v$ scaling relation parameters from

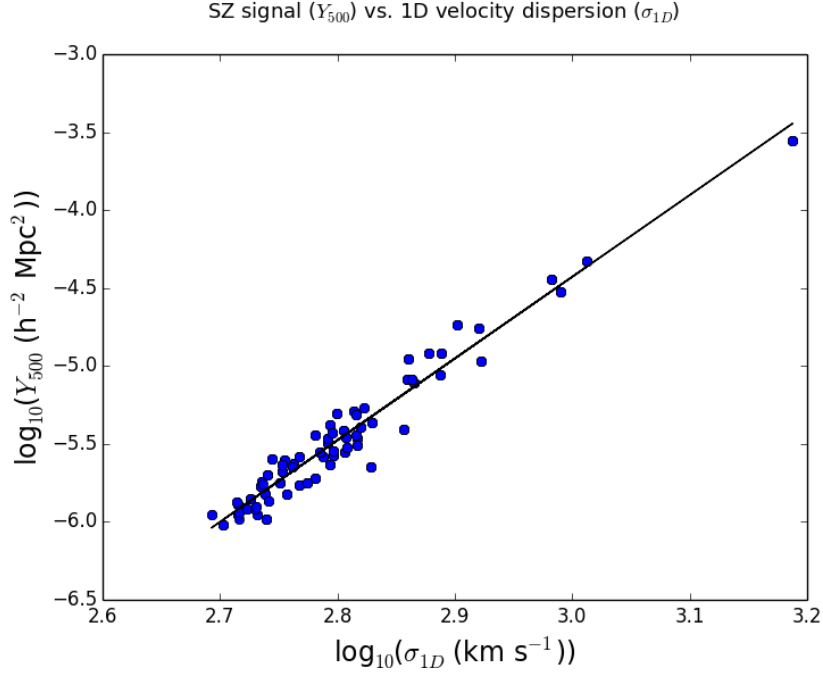


Figure 4.1: The $Y_{500}D_A^2 - \sigma_{1D}$ relation for the Millennium Gas Project simulations using the integrated SZ signal Y_{500} and the one dimensional velocity dispersion (σ_{1D}) of the total cluster mass distribution. The blue circle dots represent the cluster data within R_{500} for cluster mass $\log_{10}(M_{500}/M_{\odot}) > 13.8$, and the solid black line shows the log-log least-square best-fit line.

a Bayesian model used by Kelly (2007) for fitting a linear regression model to astronomical data that accounts for measurement errors in both the x and y-axis direction. It also allows for heteroscedastic data and intrinsic scatter in the regression relationship. The method is based on deriving a likelihood function for measured data, using a mixture of Gaussian functions which are drawn from the posterior distribution using Markov Chain Monte-Carlo (MCMC), implemented using the Gibbs sampler (e.g., see George Casella, 1992) algorithm. The MCMC simulates a random walk through the parameter space, saving the locations of the walk at each iteration which eventually converges to the posterior distribution.

Fitting $Y_{500} D_A^2 - \sigma_v$ galaxy cluster scaling relations

Here we present all the results along with methods used to find the scaling relation parameters of $Y_{500} D_A^2 - \sigma_v$. From our mock Y_{500} measurements we generated the Y_{500} errors by applying a fractional error of 0.2 that is typical of the error bars on real ACT SZ Y measurements (e.g., see [Marriage et al., 2011](#)). The 0.2 we adopted comes from the low S/N of the SZ detections, typically ~ 5 , and the size of the errors of Y_{500} vary with scale of SZ Y_{500} S/N. The mock Y_{500} measurement were scattered within the fractional error values.

To fit the scaling relation between SZ signal (Y_{500}) and the 1D velocity dispersion (σ_v), we used a Python port of the ([Kelly, 2007](#)) LINMAX-ERR IDL package (<https://github.com/jmeyers314/linmix>). The code uses a Bayesian approach to linear regression, assuming a likelihood function of the form

$$\eta_i = \alpha + \beta \xi_i + \epsilon_i \quad (4.2)$$

for the measured data, where, (α, β) , are the regression coefficients, ϵ_i is the intrinsic random scatter about the regression η_i . The values of (ξ, η) are not the actual observational measurements but instead

$$\sigma_v = \xi_i + \epsilon_{x,i} \quad (4.3)$$

and

$$Y_{500} = \eta_i + \epsilon_{y,i} \quad (4.4)$$

are the actual measurements from the mock cluster catalogue data, $\epsilon_{x,i}$ the measurement error in σ_v , and $\epsilon_{y,i}$ is the measurement error in Y_{500} . ϵ is assumed to be normally-distributed with mean zero and the variance of ϵ is assumed to be constant. The errors are also normally-distributed with known variances $\sigma_{x,i}^2$, $\sigma_{y,i}^2$ and covariance $\sigma_{xy,i}^2$. The distribution of ξ is modelled as a mixture of normals, with group proportions π , means μ , and τ^2 .

Following the assumptions of Equation 4.2, 4.3 and 4.4, a Bayesian inference is employed by running the linmix algorithm on the simulated data. The code runs ~ 1000

iterations of a MCMC to produce samples from the posterior distribution of the model, given the observed data of σ_v and Y_{500} , and it automatically compares the variance of sample parameter between chains to the variance within single chains to determine if convergence has been reached and stop. Convergence is monitored using the potential scale reduction factor (Gelman et al. 2004, described in much more detail and references therein).

The model for fitting a linear regression straight line to data that we used is described in much more detail in (Kelly, 2007, and references therein). Figure 4.2 - 4.9 show the scaling relations and fits to mock cluster samples of various sizes, observed with 1-4 slit masks. The blue dashed line is a the best fit to the data, the black circle dots represent the clusters, vertical and horizontal lines on the dots are error bars for the corresponding parameters; Y_{500} the SZ signal from MGSs integrated within R_{500} and σ_v our estimated 1D velocity dispersion. From the linear regression plots, in Figure 4.2 - 4.9, we get a scaling relation equation of this form

$$Y_{500} D_A^2 (h^{-2} \text{ Mpc}^2) = 10^{A_{rec}} \left(\frac{\sigma_v}{700 \text{ km s}^{-1}} \right)^{B_{rec}}, \quad (4.5)$$

with units ($h^{-2} \text{ Mpc}^2$) for (Y_{500}) and (km s^{-1}) for (σ_v) as shown in plots (Figure 4.2 - 4.9) and Equation 4.5 above, where A_{rec} and B_{rec} is the recovered values of the normalisation and slope respectively, 700 km s^{-1} is the pivot value of σ_v and we set the Y_{500} pivot value to 1.

Table 4.1 and 4.2 show the summary of all $Y_{500} D_A^2 - \sigma_v$ relation fit parameter results, derived from a hierarchical Bayesian model for fitting a straight line to data with error values. The 1st column shows the number of masks placed on each cluster from 1-4 respectively. The 2nd column shows the number of cluster members (N_{clus}), the 3rd and 4th column shows the recovered values of the normalisation (A_{rec}), and the slope B_{rec} along with their uncertainty measurements (AErr, BErr) for normalisation and slope respectively. The uncertainties were marginalised with 68 per cent confidence (1-sigma) on each parameter, derived using MCMC. Table 4.1 shows all the results for Figure 4.2, 4.4, 4.6 and 4.8,

where initially 26, 51, 69 and 90 clusters were randomly selected from the simulated MGSs cluster catalogue, and all the measurements were done for the sample with 100% redshift completeness. For a more realistic case we use the SALT redshift success rate and these results are all shown in Table 4.2 and Figures 4.3, 4.5, 4.7 and 4.9. The same sample of clusters was used and also same number of clusters were randomly selected clusters as in Table 4.1, the only difference being the z success rate. In the first row of Table 4.2, we can see the uncertainty on the recovered value of B_{rec} is very high, because there was no convergence on this particular set of simulated data. Clearly, observing more than 15 clusters with 1 mask is needed to constrain the slope of the $Y_{500}D_A^2 - \sigma_v$ scaling relation in a meaningful way.

Figure 4.10 and 4.11 show the ratio of the fractional difference between B_{rec} and B_{true} plotted against the number of clusters for a fixed number masks 1–4. B_{rec} represents the recovered slopes from linear regression Bayesian model fitted to simulated mock cluster data (see, Table 4.1 and 4.2 for all the parameter values of B_{rec}) and $B_{true} = 5.29$ is the slope measured directly from the MGSs cluster catalogue (see, Figure 4.1). Figure 4.10 shows that even with 100% redshift completeness, observations of more than 50 clusters are required to reduce the bias in the recovered slope to $< 10\%$. Observations of smaller samples, even with 4 masks per cluster, result in a larger bias in the recovered slope. In Figure 4.2 we can see that for the realistic case it will be reasonable to place 3 fixed masks for each of the 37 clusters, or if you have between 40 - 50 clusters to place 2–3 masks, or 1 mask for 55 clusters to have a good measurement of $Y_{500}D_A^2 - \sigma_v$ for real observations on SALT for ACT SZ selected galaxy clusters. For other measurements we can see that the fractional difference is close to 10% or more with huge uncertainty measurements. In Figure 4.11, we can see that if we have less than 37 clusters, there is a large ($\sim 30\%$) bias in the recovered slope.

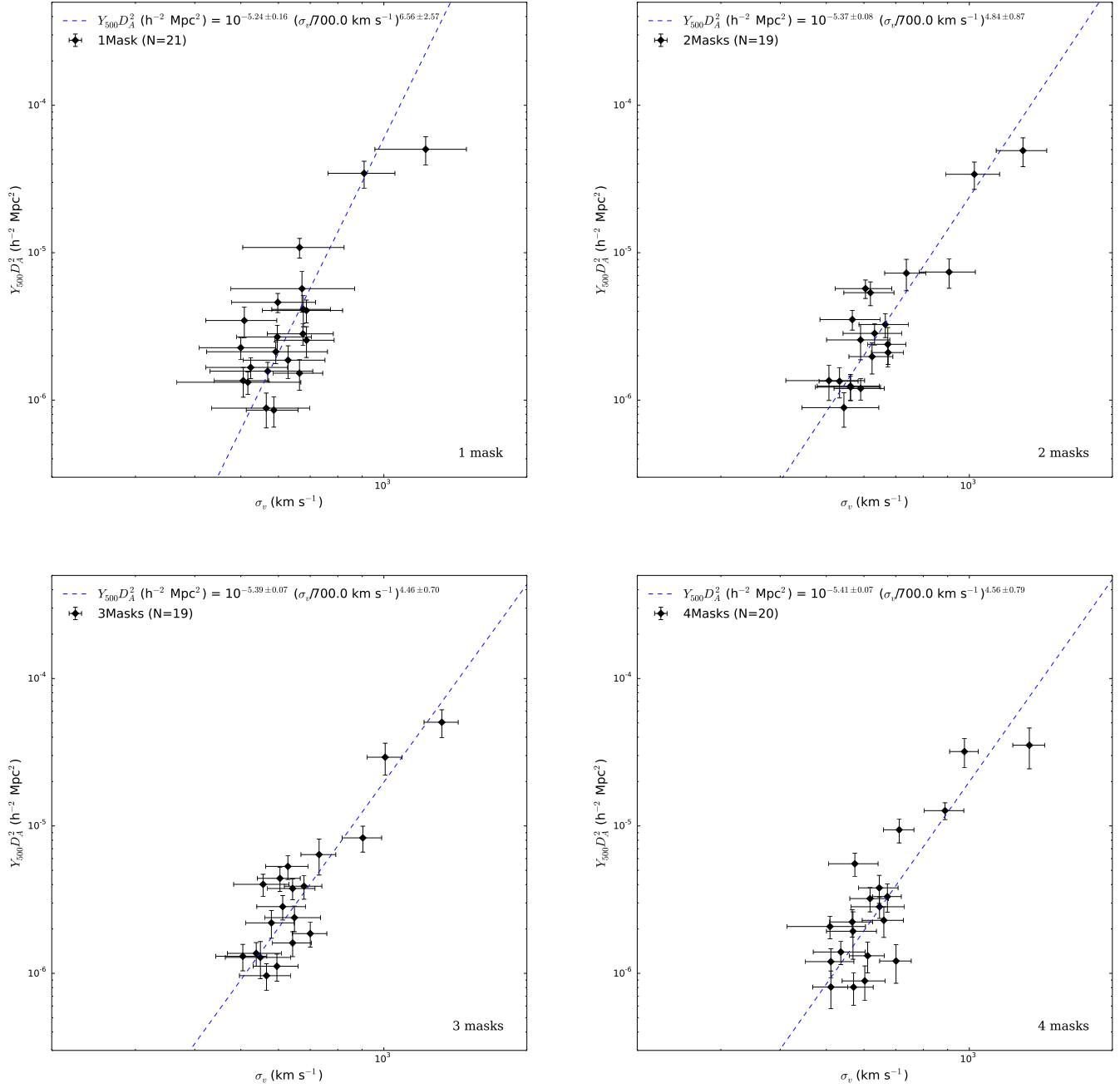


Figure 4.2: The $Y_{500}D_A^2 - \sigma_v$ scaling relation for when about 26 clusters were randomly selected initially, with 100% z completeness of all galaxies selected to be cluster members. For 1 mask, the slope is very poorly constrained, while for 2–4 mask, the uncertainty on the slope of the relation is roughly constant. N is the number of clusters in the sample. (see text for more details).

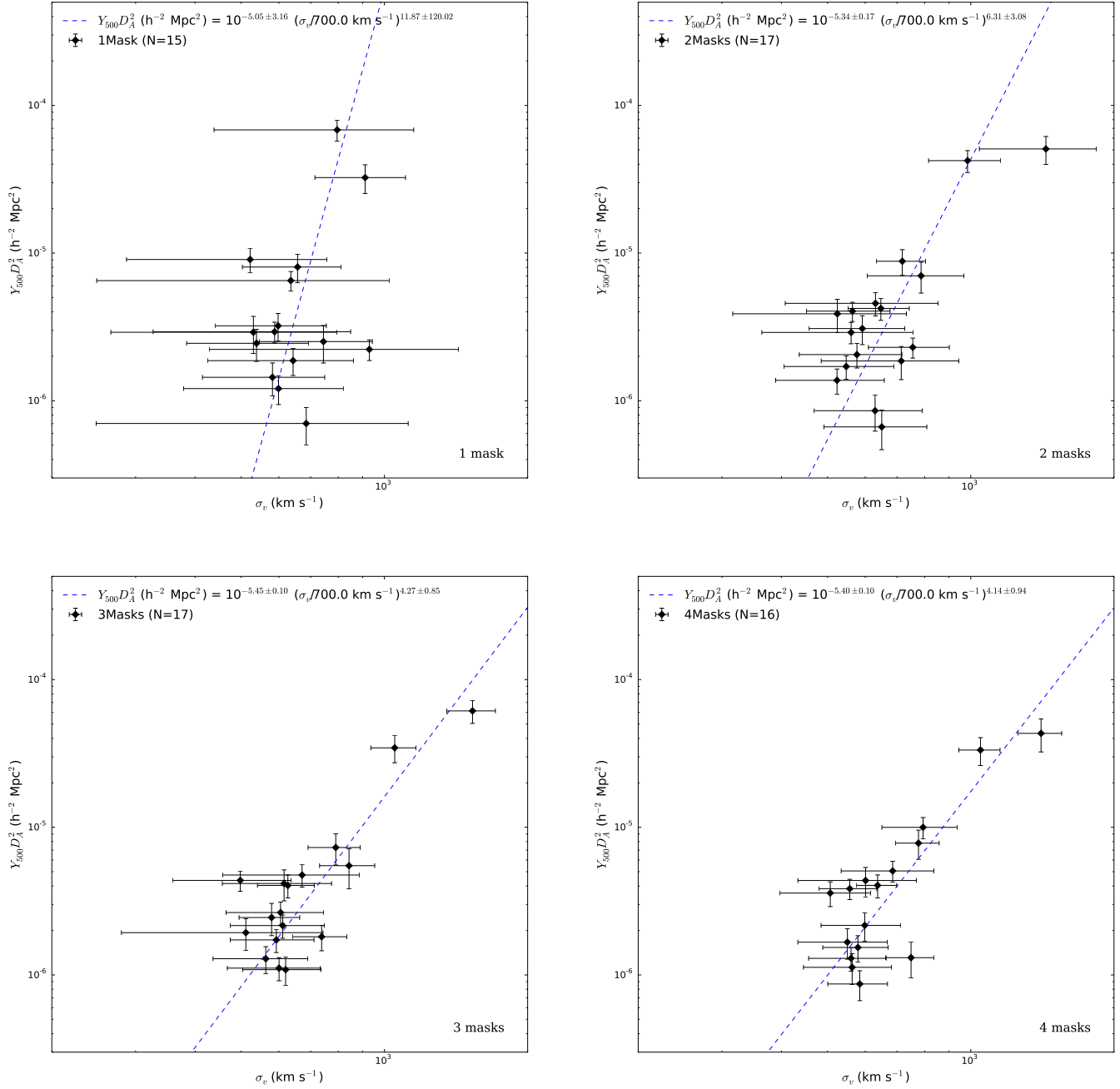


Figure 4.3: $Y_{500} D_A^2 - \sigma_v$ scaling relation for when about 26 clusters were randomly selected initially and we applied the SALT z success rate from galaxies which selected as cluster members.

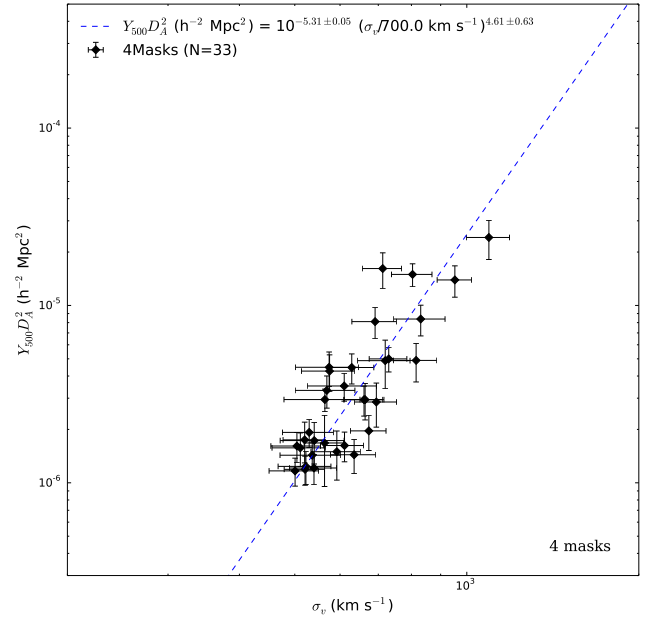
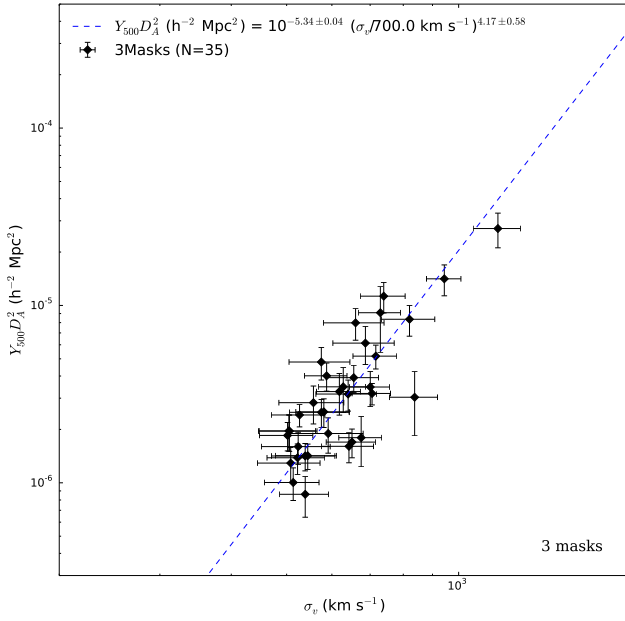
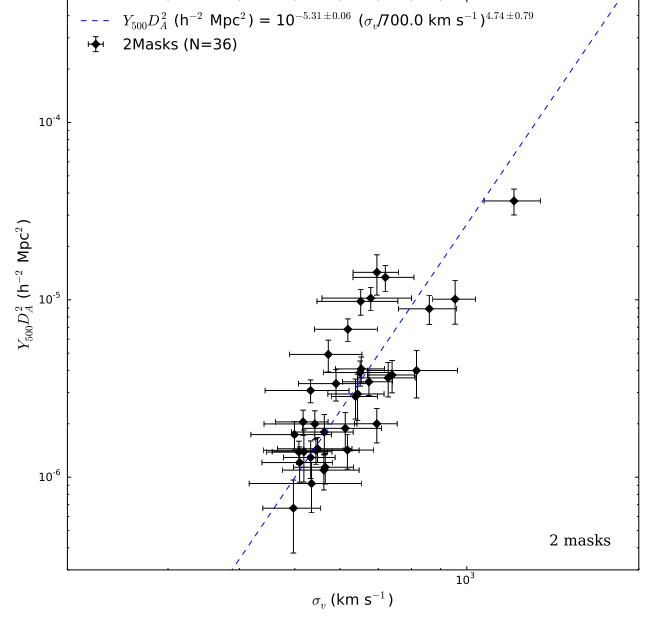
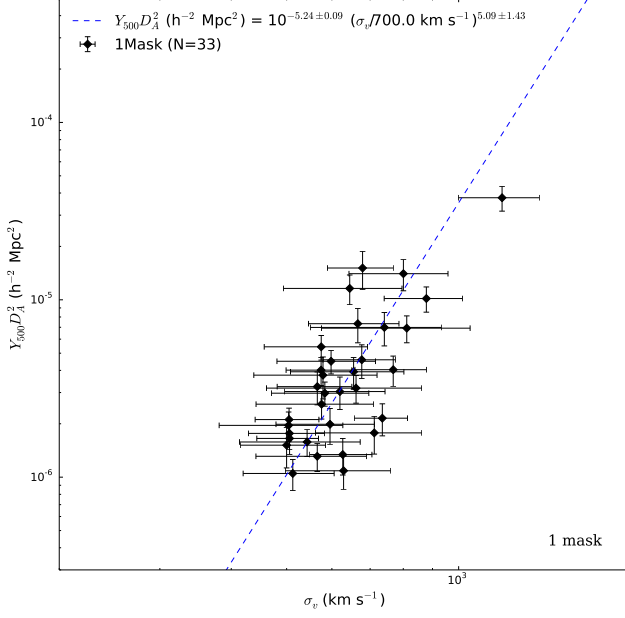


Figure 4.4: $Y_{500}D_A^2 - \sigma_v$ scaling relation for when about 51 clusters were randomly selected initially, with 100% z completeness of all galaxies selected to be cluster members.

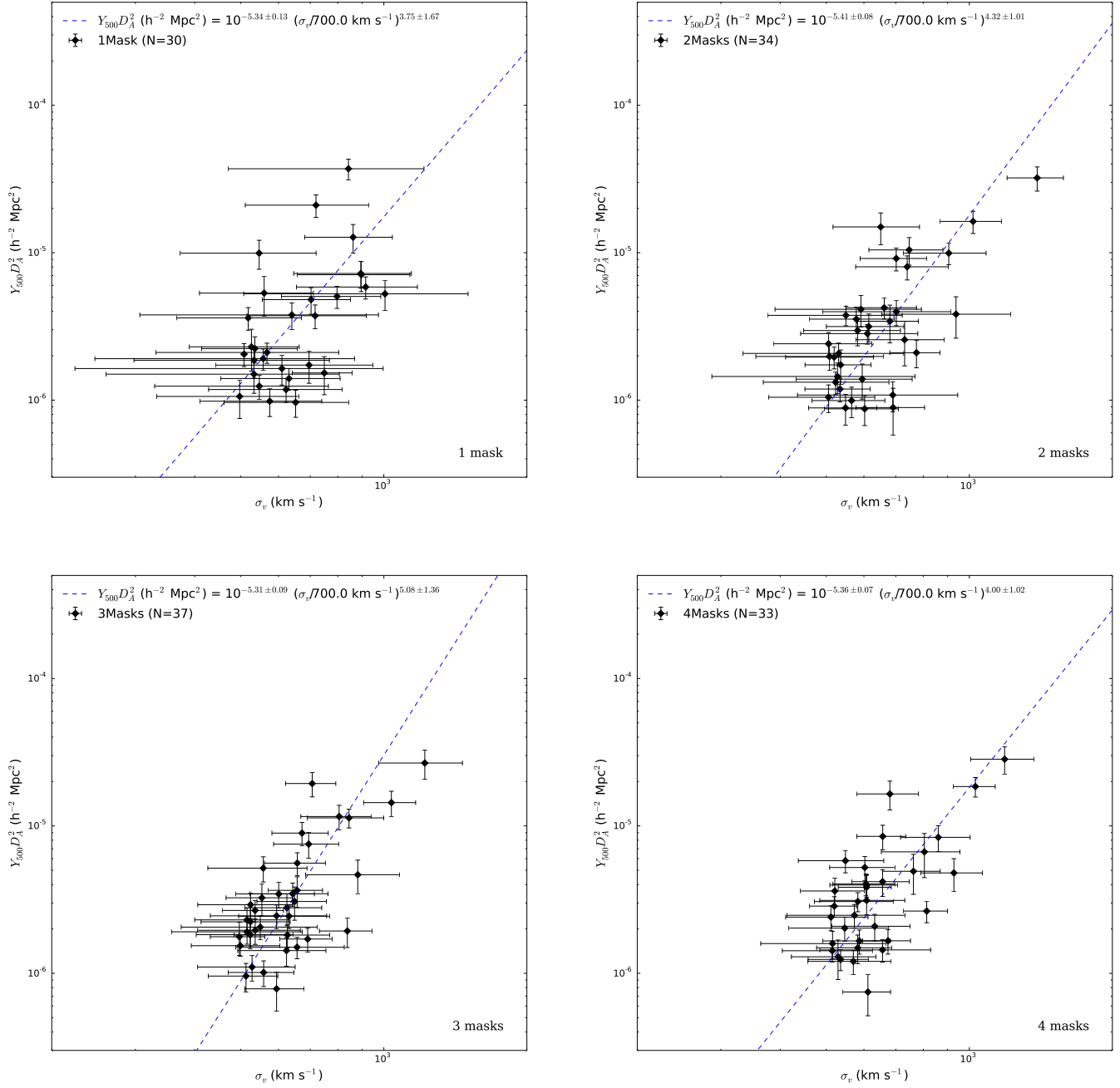


Figure 4.5: $Y_{500} D_A^2 - \sigma_v$ scaling relation for when about 51 clusters were randomly selected initially and we applied the SALT z success rate from galaxies which selected as cluster members.

Table 4.1: The best-fit $Y_{500}D_A^2 - \sigma_v$ scaling relation parameters assuming 100% redshift z completeness (see text for more details).

Masks	N_{clus}	$A \pm A\text{Err}$	$B \pm B\text{Err}$
1	21	-5.240 ± 0.163	6.564 ± 2.574
1	33	-5.242 ± 0.091	5.093 ± 1.427
1	45	-5.327 ± 0.068	5.377 ± 0.888
1	64	-5.282 ± 0.058	5.029 ± 0.656
2	19	-5.373 ± 0.078	4.840 ± 0.872
2	36	-5.309 ± 0.060	4.743 ± 0.785
2	50	-5.318 ± 0.048	5.352 ± 0.502
2	61	-5.296 ± 0.048	5.200 ± 0.607
3	19	-5.394 ± 0.066	4.458 ± 0.704
3	35	-5.335 ± 0.045	4.167 ± 0.581
3	50	-5.276 ± 0.041	5.028 ± 0.443
3	65	-5.287 ± 0.038	4.899 ± 0.477
4	20	-5.406 ± 0.073	4.560 ± 0.787
4	33	-5.314 ± 0.047	4.612 ± 0.634
4	51	-5.307 ± 0.043	4.878 ± 0.431
4	67	-5.272 ± 0.042	5.156 ± 0.536

Table 4.2: The best-fit $Y_{500}D_A^2 - \sigma_v$ scaling relation parameters, assuming redshift z completeness as a function of magnitude as in Kirk et al. (2015) where we applied the SALT redshift z success rate (see text for more details).

Masks	N_{clus}	$A \pm A\text{Err}$	$B \pm B\text{Err}$
1	15	-5.053 ± 3.162	11.874 ± 120.019
1	30	-5.338 ± 0.134	3.750 ± 1.665
1	34	-5.324 ± 0.133	6.030 ± 2.982
1	55	-5.352 ± 0.090	5.156 ± 1.119
2	17	-5.341 ± 0.172	6.306 ± 3.076
2	34	-5.415 ± 0.076	4.324 ± 1.009
2	44	-5.413 ± 0.070	5.328 ± 0.766
2	56	-5.332 ± 0.069	4.933 ± 0.842
3	17	-5.454 ± 0.096	4.266 ± 0.847
3	37	-5.307 ± 0.087	5.084 ± 1.357
3	46	-5.368 ± 0.062	5.173 ± 0.755
3	68	-5.310 ± 0.065	5.673 ± 0.879
4	16	-5.398 ± 0.099	4.135 ± 0.936
4	33	-5.358 ± 0.070	3.999 ± 1.022
4	48	-5.358 ± 0.054	4.854 ± 0.606
4	65	-5.265 ± 0.068	6.082 ± 0.927

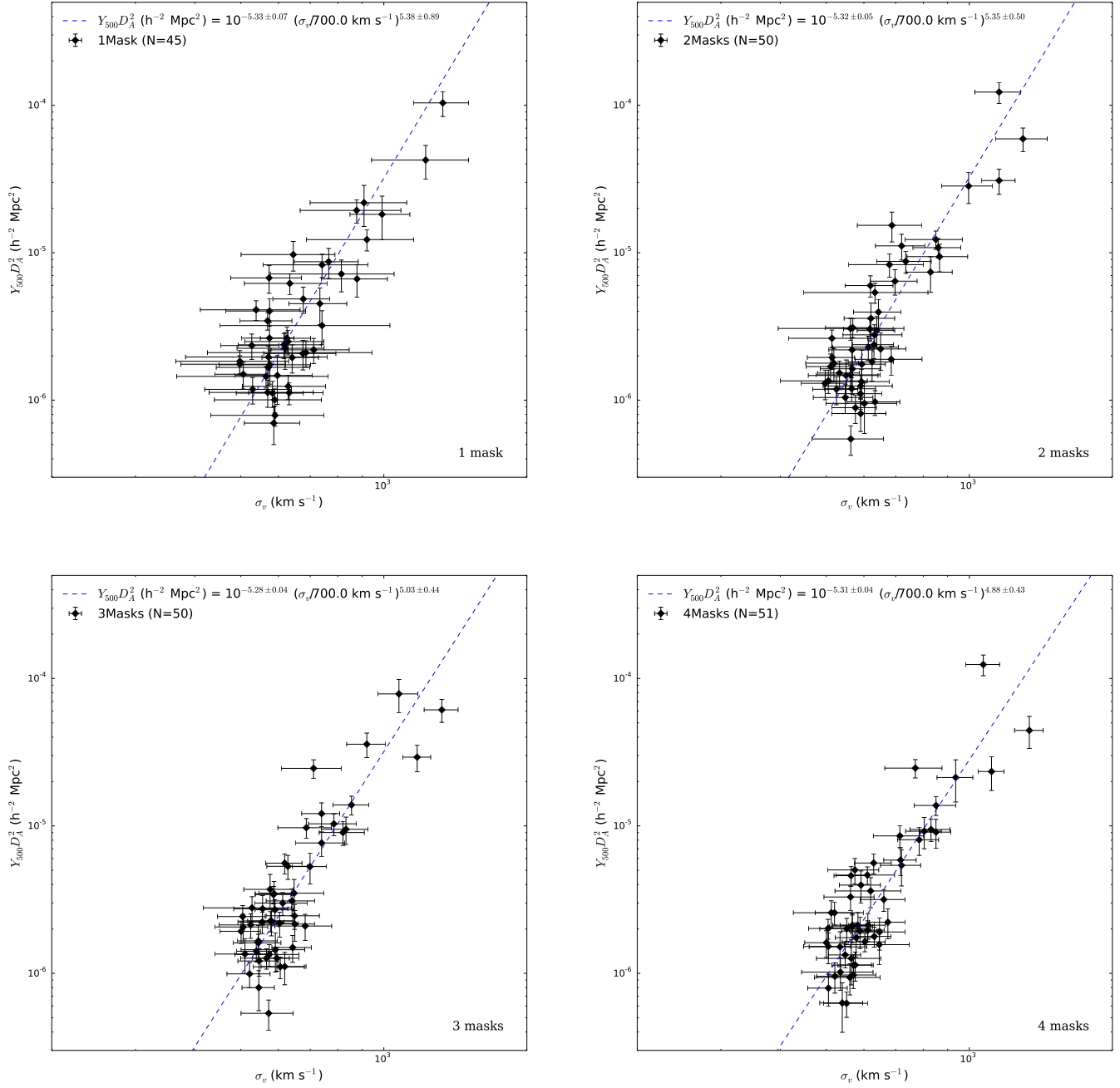


Figure 4.6: $Y_{500}D_A^2 - \sigma_v$ scaling relation for when about 69 clusters were randomly selected initially, with 100% z completeness of all galaxies selected to be cluster members.

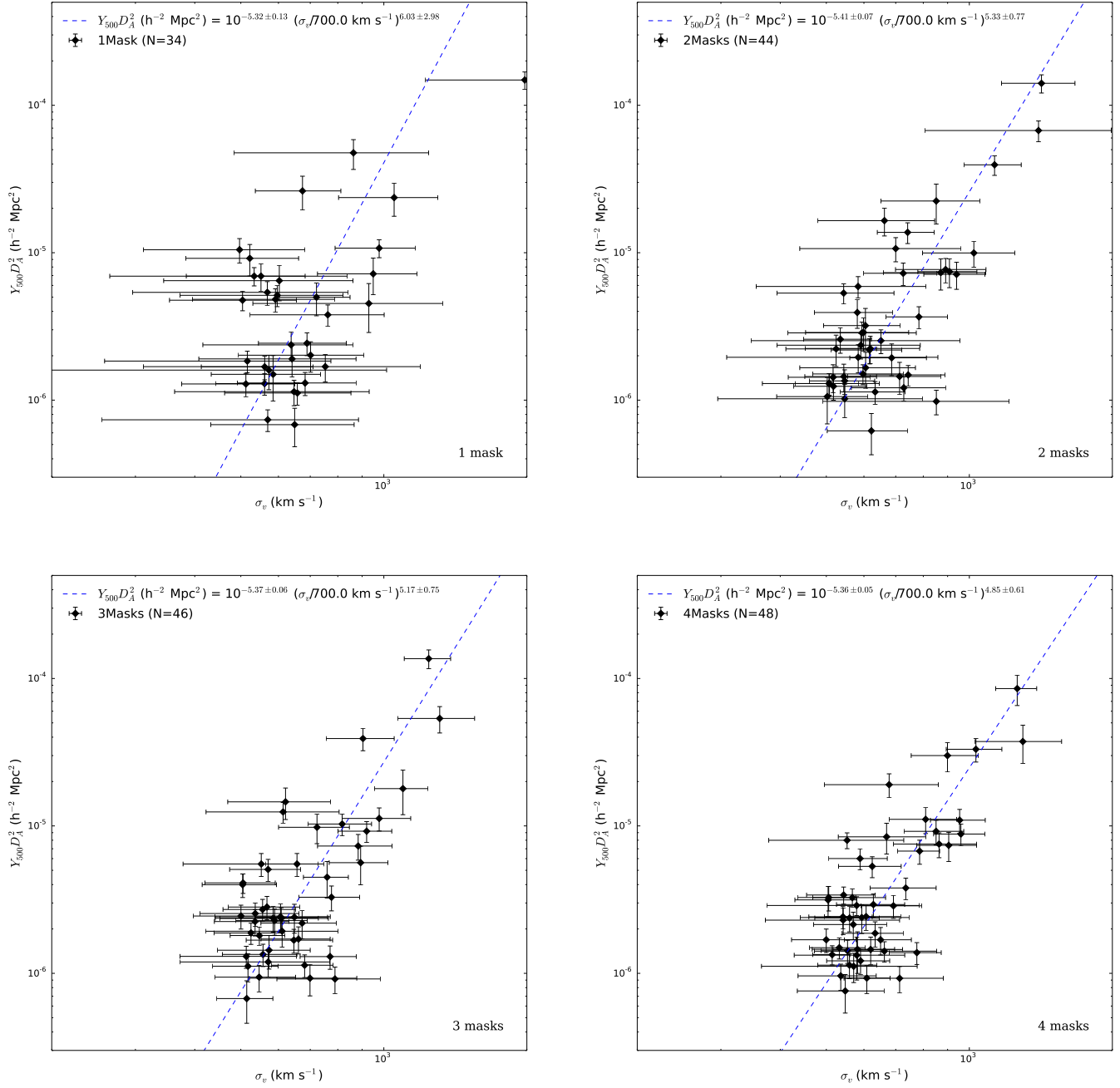


Figure 4.7: $Y_{500}D_A^2 - \sigma_v$ scaling relation for when about 69 clusters were randomly selected initially and we applied the SALT z success rate from galaxies which selected as cluster members.

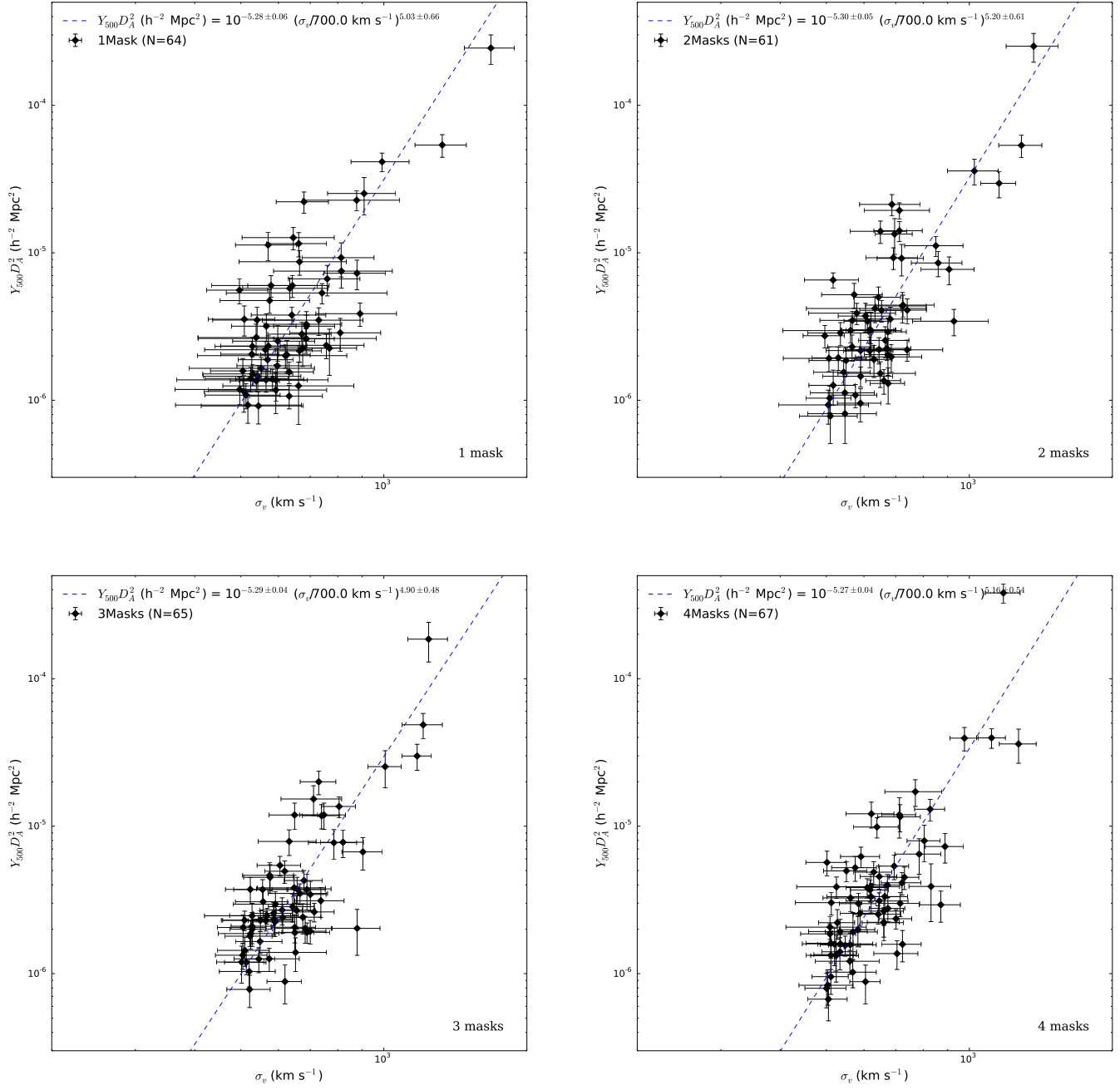


Figure 4.8: $Y_{500}D_A^2 - \sigma_v$ scaling relation for when about 90 clusters were randomly selected initially, with 100% z completeness of all galaxies selected to be cluster members.

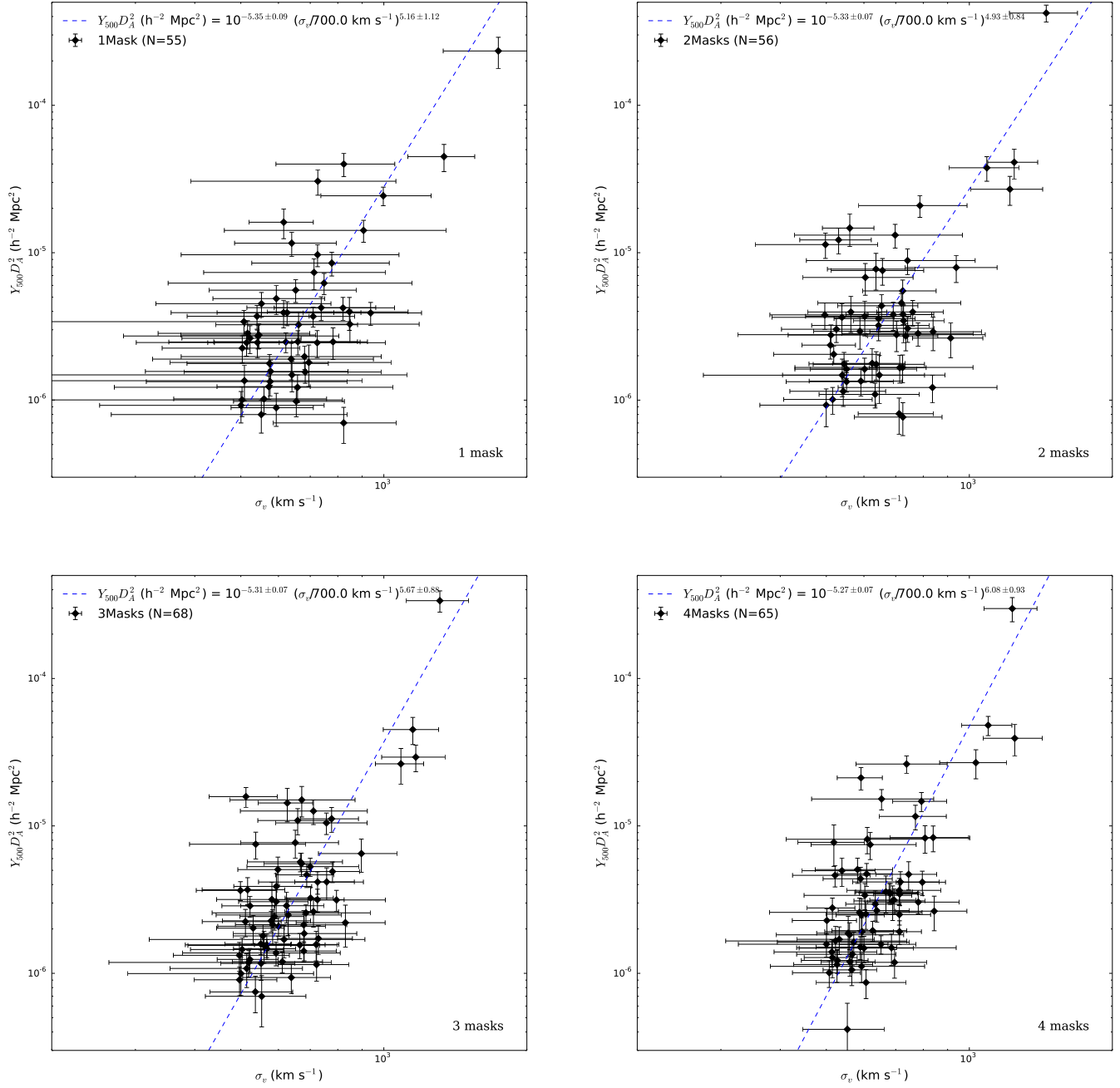


Figure 4.9: $Y_{500}D_A^2 - \sigma_v$ scaling relation for when about 90 clusters were randomly selected initially and we applied the SALT z success rate from galaxies which selected as cluster members.

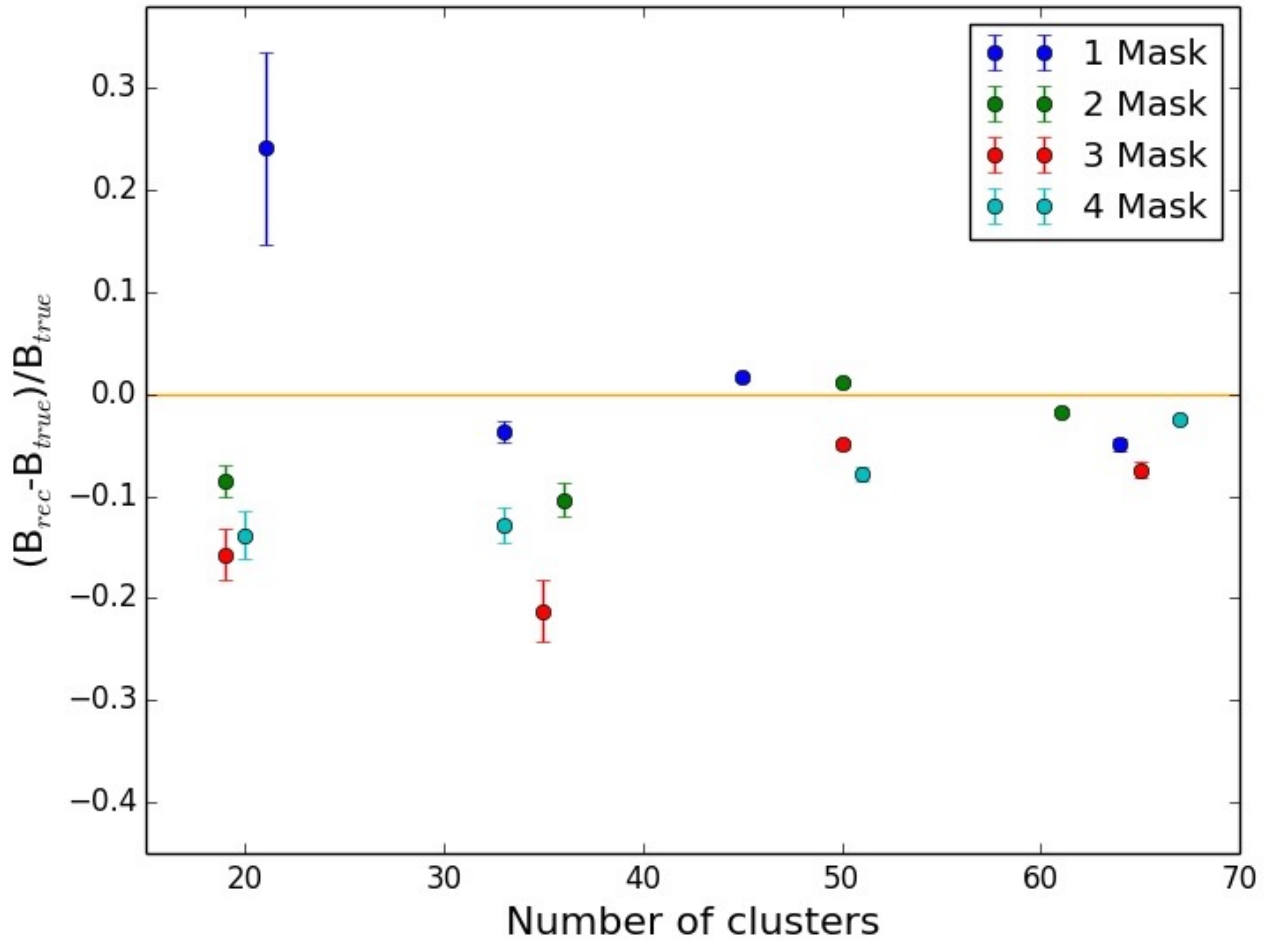


Figure 4.10: Recovery of the true slope of the $Y_{500}D_A^2 - \sigma_v$ relation as a function of the sample size, for 100% redshift completeness

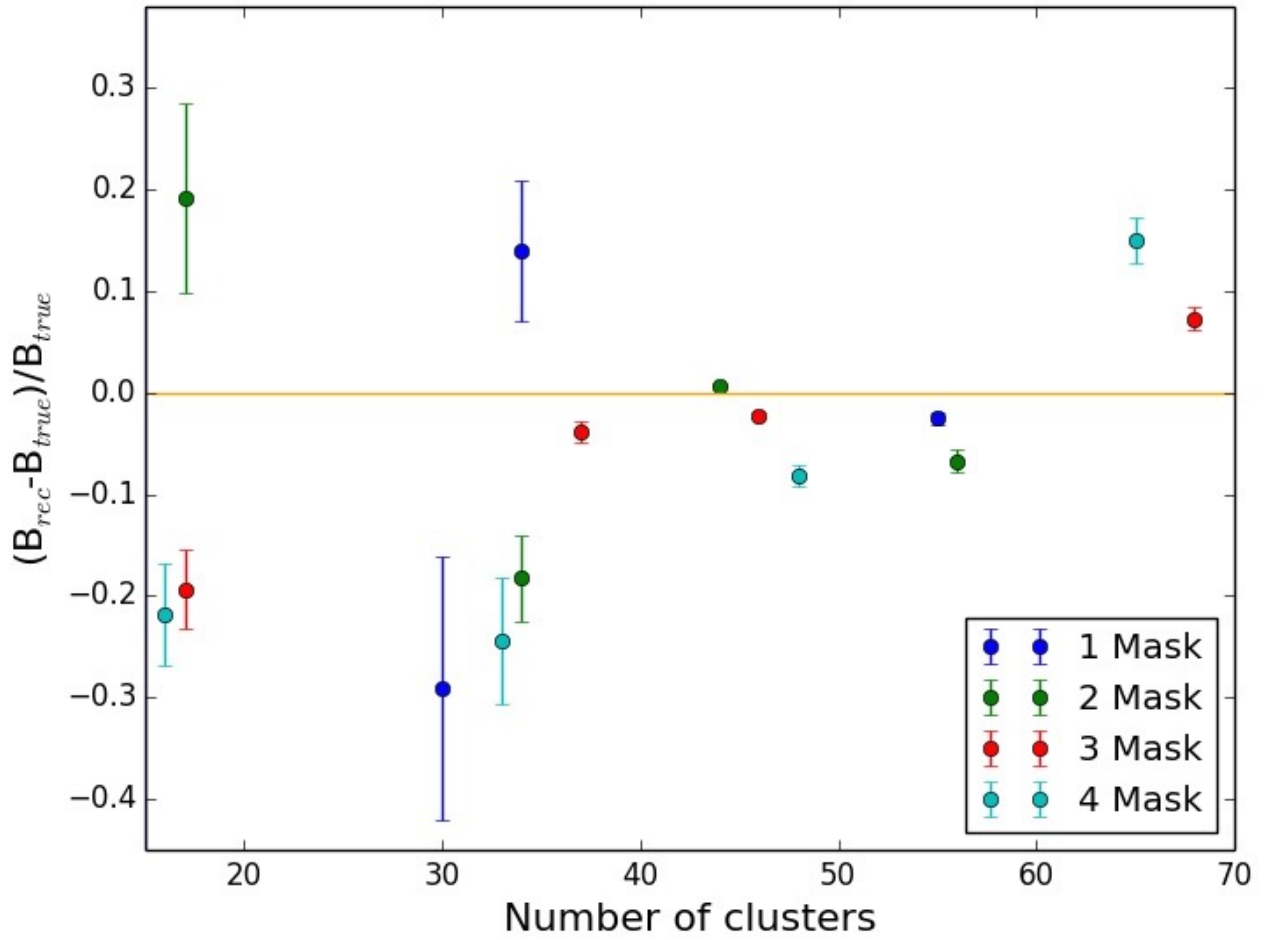


Figure 4.11: Recovery of the true slope of the $Y_{500}D_A^2 - \sigma_v$ relation as a function of the sample size, for realistic redshift completeness.

CHAPTER 5

Conclusion

Cluster of galaxies remain of great current interest due to the large number of fundamental questions concerning their formation and evolution which stand unanswered, even after many years of observational and theoretical scrutiny. The study using the SZ effect requires a well calibrated SZ - observable scaling relation in order to constrain cosmological parameters. To extract cosmological parameter estimates from cluster catalogues requires knowledge of cluster mass. Since mass is not directly observable we have to use the observable quantities as proxies to probe cluster mass. Multiple studies have highlighted the fact that the line-of-sight velocity dispersion of galaxies within clusters may be used to measure galaxy cluster masses (e.g., [Biviano et al., 2006](#); [Evrard et al., 2008](#); [Munari et al., 2013](#); [Saro et al., 2013](#); [Wilson et al., 2015](#)). The motivation to use velocity dispersion as a mass proxy for galaxy clusters stems from the fact that the galaxy dynamics are unaffected by the complex physics of the intracluster medium (ICM).

N-body/Hydrodynamic models of clusters formation and evolution have improved significantly in recent years, to a point that realistic comparisons can now be made between

theory and observations. Cluster masses can be predicted by numerical simulations of structure formation; here, we used N-body/Hydrodynamic simulations from the Millennium Gas project (MGSs; described in Section 2) to make realistic mock cluster catalogues. In Section 3.3 we explored the impact of the bias when determining cluster membership in order to make measurements of the velocity dispersion, and we found that the recovered velocity dispersion is almost unbiased (1.5–2%) but with much bigger scatter (12–20%). We then used recovered σ_v to estimate cluster dynamical mass using the scaling relation from Munari et al. (2013). We found that individual cluster mass measurements could be overestimated by up to $\sim 30\%$, but that if we applied more masks, the bias could be decreased to $\sim 11\%$.

For MOS observations, the investment of telescope time is quantised in terms of how many masks to allocate to each cluster observation. The optimisation problem is, therefore, to allocate the observation certain number of masks across a certain number clusters so as to minimize the uncertainty on the scaling relation parameters. The recovered slope (B_{rec}) is converging towards the value of true slope B_{true} as the number of cluster is increased, although there is still some bias (at the $< 10\%$ level for 100 % redshift completeness). Considering our final results (Figures 4.10 and 4.11), we conclude that for a fixed amount of telescope time, it is better to get lower quality velocity dispersion measurements for a large sample of clusters, rather than a small number of high quality observations of a small number of clusters, if the quantity of interest is the slope of the scaling relation.

Bibliography

- Abell, G. O., 1958, ‘The Distribution of Rich Clusters of Galaxies.’, *ApJS*, 3, 211–+. [12](#)
- Aihara, H., Allende Prieto, C., An, D., Anderson, S. F., Aubourg, É., Balbinot, E., Beers, T. C., et al., 2011, ‘The Eighth Data Release of the Sloan Digital Sky Survey: First Data from SDSS-III’, *ApJS*, 193, 29. [37](#)
- Allen, S. W., Evrard, A. E., Mantz, A. B., 2011, ‘Cosmological Parameters from Observations of Galaxy Clusters’, *ARA&A*, 49, 409–470. [9](#)
- Arnaud, M., Pratt, G. W., Piffaretti, R., Böhringer, H., Croston, J. H., Pointecouteau, E., 2010, ‘The universal galaxy cluster pressure profile from a representative sample of nearby systems (REXCESS) and the Y_{SZ} - M_{500} relation’, *A&A*, 517, A92. [11](#)
- Beers, T. C., Flynn, K., Gebhardt, K., 1990, ‘Measures of location and scale for velocities in clusters of galaxies - A robust approach’, *AJ*, 100, 32–46. [47](#)
- Benson, B. A., Church, S. E., all, 2004, ‘Measurements of Sunyaev-Zel’dovich Effect Scaling Relations for Clusters of Galaxies’, *ApJ*, 617, 829–846. [24](#)
- Bertone, G., 2010, ‘PARTICLE DARK MATTER Observations, Models and Searches’, *Cambridge University Press 2010*. [8](#)

- Birkinshaw, M., 1999, ‘The Sunyaev-Zel’dovich effect’, *Physics Reports*, 310, 97–195. [21](#), [24](#)
- Biviano, A., Murante, G., Borgani, S., Diaferio, A., Dolag, K., Girardi, M., 2006, ‘On the efficiency and reliability of cluster mass estimates based on member galaxies’, *A&A*, 456, 23–36. [2](#), [11](#), [71](#)
- Bleem, L. E., Stalder, B., de Haan, T., all, 2015, ‘Galaxy Clusters Discovered via the Sunyaev-Zel’dovich Effect in the 2500-Square-Degree SPT-SZ Survey’, *ApJS*, 216, 27.
- Blumenthal, G. R., Faber, S. M., Primack, J. R., Rees, M. J., 1984, ‘Formation of galaxies and large-scale structure with cold dark matter’, *Nature*, 311 (5986), 517–525.
URL <http://dx.doi.org/10.1038/311517a0> [28](#)
- Bogges, N. W., Mather, J. C., Weiss, R., all, 1992, ‘The COBE mission - Its design and performance two years after launch’, *ApJ*, 397, 420–429. [18](#)
- Borgani, S., Gardini, A., Girardi, M., Gottlöber, S., 1997, ‘Cosmology using cluster internal velocity dispersions’, *New Astronomy*, 2, 119–138. [2](#)
- Borgani, S., Murante, G., Springel, V., all, 2004, ‘X-ray properties of galaxy clusters and groups from a cosmological hydrodynamical simulation’, *MNRAS*, 348, 1078–1096. [15](#)
- Bradt, H., Mayer, W., Naranan, S., Rappaport, S., Spada, G., 1967, ‘Evidence for X-Radiation from the Radio Galaxy M87’, *ApJL*, 150, L199. [14](#)
- Byram, E. T., Chubb, T. A., Friedman, H., 1966, ‘Cosmic X-ray Sources, Galactic and Extragalactic’, *Science*, 152, 66–71. [14](#)
- Carlstrom, J. E., Ade, P. A. R., all, 2011, ‘The 10 Meter South Pole Telescope’, *PASP*, 123, 568–581. [24](#)
- Carlstrom, J. E., Holder, G. P., Reese, E. D., 2002, ‘Cosmology with the Sunyaev-Zel’dovich Effect’, *ARA&A*, 40, 643–680. [2](#), [20](#), [21](#), [23](#), [24](#)

- Catala, L., Crawford, S. M., Buckley, D. A. H., Pickering, T. E., Wilson, R. W., Butterley, T., Shepherd, H. W., Marang, F., Matshaya, P., Fourie, C., 2013, ‘Optical turbulence characterization at the SAAO Sutherland site’, *MNRAS*, 436, 590–603. [37](#)
- Cen, R., 1997, ‘Toward Understanding Galaxy Clusters and Their Constituents: Projection Effects on Velocity Dispersion, X-Ray Emission, Mass Estimates, Gas Fraction, and Substructure’, *ApJ*, 485, 39–79. [2](#)
- Crawford, S. M., Wirth, G. D., Bershad, M. A., 2014, ‘Spatial and Kinematic Distributions of Transition Populations in Intermediate Redshift Galaxy Clusters’, *ApJ*, 786, 30. [44](#)
- Davis, M., Efstathiou, G., Frenk, C. S., White, S. D. M., 1985, ‘The evolution of large-scale structure in a universe dominated by cold dark matter’, *ApJ*, 292, 371–394. [28](#)
- De Lucia, G., Blaizot, J., 2007, ‘The hierarchical formation of the brightest cluster galaxies’, *MNRAS*, 375, 2–14. [31](#)
- De Propris, R., Couch, W. J., Colless, M., Dalton, G. B., all, 2002, ‘The 2dF Galaxy Redshift Survey: a targeted study of catalogued clusters of galaxies’, *MNRAS*, 329, 87–101. [46](#)
- Duffy, A. R., Schaye, J., Kay, S. T., Dalla Vecchia, C., 2008, ‘Dark matter halo concentrations in the Wilkinson Microwave Anisotropy Probe year 5 cosmology’, *MNRAS*, 390, L64–L68. [50](#)
- Evrard, A. E., Bialek, J., Busha, M., all, 2008, ‘Virial Scaling of Massive Dark Matter Halos: Why Clusters Prefer a High Normalization Cosmology’, *ApJ*, 672, 122–137. [71](#)
- Evrard, A. E., Metzler, C. A., Navarro, J. F., 1996, ‘Mass Estimates of X-Ray Clusters’, *ApJ*, 469, 494. [15](#)

- Fadda, D., Girardi, M., Giuricin, G., Mardirossian, F., Mezzetti, M., 1996, ‘The Observational Distribution of Internal Velocity Dispersions in Nearby Galaxy Clusters’, *ApJ*, 473, 670. [44](#)
- Finn, R. A., Zaritsky, D., McCarthy, Jr., D. W., Poggianti, B., Rudnick, G., Halliday, C., Milvang-Jensen, B., Pelló, R., Simard, L., 2005, ‘H α -derived Star Formation Rates for Three $z \sim 0.75$ EDisCS Galaxy Clusters’, *ApJ*, 630, 206–227. [46](#)
- Fixsen, D. J., Cheng, E. S., Gales, J. M., all, 1996, ‘The Cosmic Microwave Background Spectrum from the Full COBE FIRAS Data Set’, *ApJ*, 473, 576. [18](#)
- Forman, W., Jones, C., Cominsky, L., Julien, P., Murray, S., Peters, G., Tananbaum, H., Giacconi, R., 1978, ‘The fourth Uhuru catalog of X-ray sources.’, *ApJS*, 38, 357–412. [14](#)
- Freedman, W. L., Madore, B. F., Gibson, B. K., Ferrarese, L., Kelson, D. D., Sakai, S., Mould, J. R., Kennicutt, Jr., R. C., Ford, H. C., Graham, J. A., Huchra, J. P., Hughes, S. M. G., Illingworth, G. D., Macri, L. M., Stetson, P. B., 2001, ‘Final Results from the Hubble Space Telescope Key Project to Measure the Hubble Constant’, *ApJ*, 553, 47–72. [5](#), [7](#)
- Gamow, G., 1946, ‘Expanding Universe and the Origin of Elements’, *Physical Review Letters*, 70, 572–573. [16](#)
- George Casella, E. I. G., 1992, ‘Explaining the gibbs sampler’, *American Statistical Association, Taylor & Francis, Ltd.*, 46 (3), 167–174. [55](#)
- Grego, L., Carlstrom, J. E., Reese, E. D., all, 2001, ‘Galaxy Cluster Gas Mass Fractions from Sunyaev-Zeldovich Effect Measurements: Constraints on Ω_M ’, *ApJ*, 552, 2–14. [24](#)
- Gunn, J. E., Siegmund, W. A., Mannery, E. J., et al., 2006, ‘The 2.5 m Telescope of the Sloan Digital Sky Survey’, *AJ*, 131, 2332–2359. [36](#)

- Hartley, W. G., Gazzola, L., Pearce, F. R., Kay, S. T., Thomas, P. A., 2008, ‘Nature versus nurture: the curved spine of the galaxy cluster X-ray luminosity-temperature relation’, *MNRAS*, 386, 2015–2021. [29](#)
- Hasselfield, M., Hilton, M., Marriage, T. A., et al., 2013a, ‘The Atacama Cosmology Telescope: Sunyaev-Zel’dovich selected galaxy clusters at 148 GHz from three seasons of data’, *JCAP*, 7, 8. [2](#), [24](#), [35](#), [37](#)
- Hasselfield, M., et al., 2013b, ‘The Atacama Cosmology Telescope: Sunyaev-Zel’dovich selected galaxy clusters at 148 GHz from three seasons of data’, *JCAP*, 7, 8.
- Hoekstra, H., Bartelmann, M., Dahle, H., Israel, H., Limousin, M., Meneghetti, M., 2013, ‘Masses of Galaxy Clusters from Gravitational Lensing’, *Space Science Reviews*, 177, 75–118. [11](#)
- Hubble, E., 1929, ‘A Relation between Distance and Radial Velocity among Extra-Galactic Nebulae’, *Proceedings of the National Academy of Sciences of the United States of America*, 15, 168–173. [4](#)
- Kay, S. T., Peel, M. W., Short, C. J., Thomas, P. A., Young, O. E., Battye, R. A., Liddle, A. R., Pearce, F. R., 2012, ‘Sunyaev-Zel’dovich clusters in Millennium gas simulations’, *MNRAS*, 422, 1999–2023. [2](#), [11](#), [29](#), [31](#), [32](#), [33](#), [34](#), [41](#), [54](#)
- Kelly, B. C., 2007, ‘Some Aspects of Measurement Error in Linear Regression of Astronomical Data’, *ApJ*, 665, 1489–1506. [55](#), [56](#), [57](#)
- Kirk, B., Hilton, M., Cress, C., Crawford, S. M., et al., 2015, ‘SALT spectroscopic observations of galaxy clusters detected by ACT and a type II quasar hosted by a brightest cluster galaxy’, *MNRAS*, 449, 4010–4026. [2](#), [35](#), [36](#), [37](#), [38](#), [39](#), [40](#), [42](#), [43](#), [44](#), [47](#)
- Komatsu, E., et al., 2011, ‘Seven-year Wilkinson Microwave Anisotropy Probe (WMAP) Observations: Cosmological Interpretation’, *ApJS*, 192, 18. [1](#), [6](#)

- Kravtsov, A. V., Borgani, S., 2012, ‘Formation of Galaxy Clusters’, *ARA&A*, 50, 353–409. [11](#)
- Kurtz, M. J., Mink, D. J., 1998, ‘RVSAO 2.0: Digital Redshifts and Radial Velocities’, *PASP*, 110, 934–977. [38](#)
- Liddle, A., 2010, ‘An Introduction to Modern Cosmology’. [11](#), [16](#)
- Lucy, L. B., 1983, ‘The formation of resonance lines in locally nonmonotonic winds. II - an amplitude diagnostic’, *ApJ*, 274, 372–379. [2](#)
- Mamon, G. A., Biviano, A., Murante, G., 2010, ‘The universal distribution of halo interlopers in projected phase space. Bias in galaxy cluster concentration and velocity anisotropy?’, *A&A*, 520, A30. [2](#)
- Marriage, T. A., et al., 2011, ‘The Atacama Cosmology Telescope: Sunyaev-Zel’dovich-Selected Galaxy Clusters at 148 GHz in the 2008 Survey’, *ApJ*, 737, 61. [20](#), [56](#)
- Mathiesen, B. F., Evrard, A. E., 2001, ‘Four Measures of the Intracluster Medium Temperature and Their Relation to a Cluster’s Dynamical State’, *ApJ*, 546, 100–116. [15](#)
- Melott, A. L., Einasto, J., Saar, E., Suisalu, I., Klypin, A. A., Shandarin, S. F., 1983, ‘Cluster analysis of the nonlinear evolution of large-scale structure in an axion/gravitino/photino-dominated universe’, *Physical Review Letters*, 51, 935–938. [28](#)
- Menanteau, F., Sifón, C., Barrientos, L. F., et al., 2013, ‘The Atacama Cosmology Telescope: Physical Properties of Sunyaev-Zel’dovich Effect Clusters on the Celestial Equator’, *ApJ*, 765, 67. [2](#), [24](#), [35](#), [37](#)
- Mo, H., Van Den Bosch, F., White, S., 2010, ‘Galaxy Formation and Evolution’, *Cambridge University Press*. [5](#)
- Munari, E., Biviano, A., Borgani, S., Murante, G., Fabjan, D., 2013, ‘The relation between velocity dispersion and mass in simulated clusters of galaxies: dependence on the tracer and the baryonic physics’, *MNRAS*, 430, 2638–2649. [42](#), [43](#), [49](#), [53](#), [71](#), [72](#)

- Navarro, J. F., Frenk, C. S., White, S. D. M., 1997, ‘A Universal Density Profile from Hierarchical Clustering’, *ApJ*, 490, 493. [50](#)
- Padin, S., Staniszewski, Z., all, 2008, ‘South Pole Telescope optics’, *Optical Society of America*, 47, 4418 – 4428. [24](#)
- Padmanabhan, T., et al., 1993, ‘Structure Formation in the Universe series volume 1’, *Cambridge University Press*. [8](#)
- Penzias, A. A., Wilson, R. W., 1965, ‘A Measurement of Excess Antenna Temperature at 4080 Mc/s.’, *ApJ*, 142, 419–421. [16](#)
- Perlmutter, S., Aldering, G., Goldhaber, G., et al., 1999, ‘Measurements of Ω and Λ from 42 High-Redshift Supernovae’, *ApJ*, 517, 565–586. [5](#)
- Planck Collaboration, Ade, P. A. R., Aghanim, N., Armitage-Caplan, C., Arnaud, M., Ashdown, M., Atrio-Barandela, F., Aumont, J., Aussel, H., Baccigalupi, C., et al., 2014, ‘Planck 2013 results. XXIX. The Planck catalogue of Sunyaev-Zeldovich sources’, *A&A*, 571, A29. [20](#), [24](#)
- Planck Collaboration, Ade, P. A. R., Aghanim, N., Arnaud, M., Ashdown, M., Aumont, J., Baccigalupi, C., Banday, A. J., Barreiro, R. B., Bartlett, J. G., et al., 2015, ‘Planck 2015 results. XIII. Cosmological parameters’, *A&A*. [3](#)
- Planck Collaboration, Aghanim, N., all, 2011, ‘Planck early results. IX. XMM-Newton follow-up for validation of Planck cluster candidates’, *A&A*, 536, A9. [32](#), [34](#)
- Popesso, P., Biviano, A., Böhringer, H., Romaniello, M., 2007, ‘RASS-SDSS galaxy cluster survey. VII. On the cluster mass-to-light ratio and the halo occupation distribution’, *A&A*, 464, 451–464. [11](#)
- Primack, J. R., Blumenthal, G. R., 1984, ‘What is the dark matter? - Implications for galaxy formation and particle physics’, In: Audouze, J., Tran Thanh Van, J. (Eds.),

- NATO Advanced Science Institutes (ASI) Series C, Vol. 117 of *NATO Advanced Science Institutes (ASI) Series C*, pp. 163–183. [28](#)
- Riess, A. G., Filippenko, A. V., Challis, P., et al., 1998, ‘Observational Evidence from Supernovae for an Accelerating Universe and a Cosmological Constant’, *AJ*, 116, 1009–1038. [5](#)
- Roos, M., 2008, ‘Expansion of the Universe - Standard Big Bang Model’, *John Wiley & Sons, Ltd.* [3](#)
- Rosati, P., Borgani, S., Norman, C., 2002, ‘The Evolution of X-ray Clusters of Galaxies’, *ARA&A*, 40, 539–577. [15](#), [16](#)
- Rykoff, E. S., Rozo, E., Busha, M. T., Cunha, C. E., Finoguenov, A., Evrard, A., Hao, J., Koester, B. P., Leauthaud, A., Nord, B., Pierre, M., Reddick, R., Sadibekova, T., Sheldon, E. S., Wechsler, R. H., 2014, ‘redMaPPer. I. Algorithm and SDSS DR8 Catalog’, *ApJ*, 785, 104. [12](#), [37](#)
- Sarazin, C. L., et al., 1988, ‘Cambridge Astrophysics Series’, *Cambridge University Press.* [10](#), [15](#)
- Saro, A., Mohr, J. J., Bazin, G., Dolag, K., 2013, ‘Toward Unbiased Galaxy Cluster Masses from Line-of-sight Velocity Dispersions’, *ApJ*, 772, 47. [11](#), [71](#)
- Schechter, P., 1976, ‘An analytic expression for the luminosity function for galaxies.’, *ApJ*, 203, 297–306. [13](#)
- Short, C. J., Thomas, P. A., 2009, ‘Combining Semianalytic Models with Simulations of Galaxy Clusters: The Need for Heating from Active Galactic Nuclei’, *ApJ*, 704, 915–929.
- Short, C. J., Thomas, P. A., Young, O. E., Pearce, F. R., Jenkins, A., Muanwong, O., 2010, ‘The evolution of galaxy cluster X-ray scaling relations’, *MNRAS*, 408, 2213–2233. [29](#), [31](#), [32](#), [41](#)

- Sifón, C., et al., 2013, ‘The Atacama Cosmology Telescope: Dynamical Masses and Scaling Relations for a Sample of Massive Sunyaev-Zel’dovich Effect Selected Galaxy Clusters’, *ApJ*, 772, 25. [24](#), [25](#)
- Spergel, D. N., Verde, L., Peiris, H. V., Komatsu, E., Nolta, M. R., Bennett, C. L., Halpern, M., Hinshaw, G., Jarosik, N., Kogut, A., Limon, M., Meyer, S. S., Page, L., Tucker, G. S., Weiland, J. L., Wollack, E., Wright, E. L., 2003, ‘First-Year Wilkinson Microwave Anisotropy Probe (WMAP) Observations: Determination of Cosmological Parameters’, *ApJS*, 148, 175–194. [29](#)
- Springel, V., 2005, ‘The cosmological simulation code GADGET-2’, *MNRAS*. [29](#)
- Springel, V., White, S. D. M., Jenkins, A., Frenk, C. S., et al., 2005, ‘Simulations of the formation, evolution and clustering of galaxies and quasars’, *Nature*, 435, 629–636. [28](#), [29](#), [31](#)
- Stanek, R., Rasia, E., Evrard, A. E., Pearce, F., Gazzola, L., 2010, ‘Massive Halos in Millennium Gas Simulations: Multivariate Scaling Relations’, *ApJ*, 715, 1508–1523. [31](#)
- Stanek, R., Rudd, D., Evrard, A. E., 2009, ‘The effect of gas physics on the halo mass function’, *MNRAS*, 394, L11–L15. [29](#)
- Staniszewski, Z., Ade, P. A. R., et al., 2009, ‘Galaxy Clusters Discovered with a Sunyaev-Zel’dovich Effect Survey’, *ApJ*, 701, 32–41. [24](#)
- Sunyaev, R. A., Zeldovich, Y. B., 1972, ‘The Observations of Relic Radiation as a Test of the Nature of X-Ray Radiation from the Clusters of Galaxies’, *Comments on Astrophysics and Space Physics*, 4, 173. [18](#)
- Swetz, D. S., et al., 2011, ‘Overview of the Atacama Cosmology Telescope: Receiver, Instrumentation, and Telescope Systems’, *ApJS*, 194, 41. [2](#), [24](#)
- van den Bergh, S., 1976, ‘A new classification system for galaxies’, *ApJ*, 206, 883–887. [6](#)

- Vanderlinde, K., Crawford, T. M., de Haan, T., et al., 2010, ‘Galaxy Clusters Selected with the Sunyaev-Zel’dovich Effect from 2008 South Pole Telescope Observations’, *ApJ*, 722, 1180–1196. [20](#)
- Vikhlinin, A., Burenin, R. A., Ebeling, H., et al., 2008, ‘Chandra Cluster Cosmology Project. II. Samples and X-Ray Data Reduction’, *ApJ*, 692, 1033–1059. [15](#)
- Vikhlinin, A., Kravtsov, A. V., Burenin, R. A., Ebeling, H., Forman, W. R., Hornstrup, A., Jones, C., Murray, S. S., Nagai, D., Quintana, H., Voevodkin, A., 2009, ‘Chandra Cluster Cosmology Project III: Cosmological Parameter Constraints’, *ApJ*, 692, 1060–1074. [9](#), [10](#)
- Voit, G. M., 2005, ‘Tracing cosmic evolution with clusters of galaxies’, *Reviews of Modern Physics*, 77, 207–258. [13](#)
- Williamson, R., Benson, B. A., High, F. W., et al., 2011, ‘A Sunyaev-Zel’dovich-selected Sample of the Most Massive Galaxy Clusters in the 2500 deg² South Pole Telescope Survey’, *ApJ*, 738, 139. [11](#)
- Wilson, S., Hilton, M., Rooney, P. J., Caldwell, C., et al., 2015, ‘The XMM Cluster Survey: evolution of the velocity dispersion – temperature relation over half a Hubble time’, *MNRAS*. [42](#), [44](#), [47](#), [71](#)
- Wojtak, R., Lokas, E. L., Mamon, G. A., Gottlöber, S., Prada, F., Moles, M., 2007, ‘Interloper treatment in dynamical modelling of galaxy clusters’, *A&A*, 466, 437–449. [2](#)
- Yoo, J., Watanabe, Y., 2012, ‘Theoretical Models of Dark Energy’, *ijmp*, 21, 1230002. [6](#)
- Young, O. E., Thomas, P. A., Short, C. J., Pearce, F., 2011, ‘Baryon fractions in clusters of galaxies: evidence against a pre-heating model for entropy generation’, *MNRAS*, 413, 691–704. [29](#)